CHAPTER 6: ETOPOSIDE

CHAPTER-6: ETOPOSIDE

6.1 Introduction:

Etoposide (ETO) is a less toxic and more effective semi-synthetic derivative of podophyllotoxin(1). Anti-mitotic properties of podophyllin was established in as early as 1946(2). It is widely used for treatment of AML (Acute myeloid leukaemia), Hodgkin's disease, non-Hodgkin's lymphoma and cancers of gastric, lung, prostate, ovary and testes. The main mechanism of action involves inhibition of Topoisomerase II enzyme and prevention of DNA re-ligation. These faults or breaks in DNA leads to killing of cancer cells. It has been proved to cause dose-dependent single strand and double strand DNA breaks(3). The topoisomerase II enzymes are responsible for regulating under winding and over winding of the DNA strands thus solving nucleic acid knots and tangles(4, 5). Etoposide poisons these enzymes by increasing the steady state concentration of the covalent DNA cleavage complexes, thus converting Topoisomerases into physiological toxins that introduce transient protein associated breaks in the genome of treated cells. The breaks introduced prevent recombination, sister chromatid exchange , promotes large insertions and deletions , producing chromosomal aberrations and translocation. The accumulation of permanent breaks in sufficient concentration leads to ultimate cell death by apoptosis(1).

ETO comes under the Biopharmaceutics classification system (BCS) class IV and suffers from solubility as well as permeability limitations. This leads to solubility and bioavailability issues. Formulating a novel drug delivery system can help in addressing various issues related to this drug. In this research work, an extensive investigation was carried out to determine the efficacy of mesoporous silica nanoparticles MCM-41 in particular in functioning as a delivery system for ETO. Their impact on the solubility and bioavailability of the drug was assessed. For oral delivery unfunctionalized MSNs and amine functionalized MSNs both were tested and comparison was made to determine effect of functionalization on ETO release and efficacy.

Mesoporous silica nanoparticles were selected due to the various advantages associated with them like zero premature leakage(6), excellent chemical and thermal stability(7), tunable pore size with large surface area(8), and ease of surface functionalization with good biocompatibility(9).

Surface functionalized MCM-41 nanocarriers were investigated for their targeting efficacy so that ETO can exclusively reach cancer cells and its side effects on healthy cells can be avoided. For this purpose stimuli responsive and receptor based delivery system was designed. Stimuli based system was based on internal stimuli exploiting difference in the immediate environment of the cancer cells and normal cells. The extracellular tumour pH value is 6.8 (10) and endosomal pH is 5.5 (11)both lower than that of normal cells with pH 7.4. Cancer cells survive or possess an acidic environment and hence it was thought of interest to investigate a pH based MSN delivery system for ETO and determine their targeting efficiency. For this purpose Polyacrylic acid (PAA) was used as a pH responsive polymer and a facile approach was used for its attachment onto MSNs. PAA was selected based on certain advantages associated with it like completely biodegradable, minimal toxicity, carboxylic group and eccentric physicochemical properties imparting more hydrophilicity to MSNs(12, 13). It has been employed as a pH responsive carrier in various studies(14-16). Furthermore, both the qualitative and qualitative cellular uptake were determined for PAA-MSNs along with the pharmacokinetic evaluation and biodistribution studies in male swiss albino mice.

A second approach used was targeting of certain receptors overexpressed in cancer cells. For this approach Folic acid ligand was used and decorated onto MSN surface to target the overexpressed folic acid receptors of cancer cells. Prostate cancer cells have been known to overexpress folate binding proteins on their membrane(17-19). Only few studies have been reported so far studying the folate targeting in prostate cancer(20, 21) and lots still remains to be explored. However no mesoporous folic acid functionalised formulation was reported so far

and hence an investigation of how folate functionalized MSNs were useful in cell specific or targeted prostate cancer treatment was undertaken. The cell death mechanism, cell killing efficiency and cellular uptake was determined. Furthermore, hemocompatibility biodistribution and histological examination was carried out to ensure the safety aspects of synthesized MSNs.

Thus, in the present chapter the application of bare and functionalized MSNs as oral as well as intravenous targeted delivery agents for ETO in cancer therapy have been discussed in depth along with their biosafety aspects and efficacy.

6.2 Materials and methods:

6.2.1 Chemicals and reagents

Pure anhydrous active pharmaceutical ingredient (API) Etoposide (ETO) was obtained as a sample gratis from Intas Pharmaceuticals Ltd, (Ahmedabad, Gujarat, India). Tapentadol (TAP) was kindly gifted by Ami life sciences ltd , Vadodara, Gujarat.

Chemicals required for preparation of dissolution media viz, hydrochloric acid, sodium acetate trihydrate, acetic acid, monobasic potassium phosphate, sodium chloride, ammonium acetate and potassium dihydrogen phosphate were purchased from S.D. Fine Chem Ltd, Mumbai. Vital ingredients like pancreatin, pepsin, sodium taurocholate and Lecithin were obtained from Sigma Aldrich (St. Louis, USA). For diffusion study, dialysis tubes having cut-off Molecular weights (Mw) of 7000 g/mol and 3500 g/mol were purchased from HImedia laboratories, Mumbai.

Fluorescein isothiocyanate (FITC) and 4,6-Diamidino-2-Phenylindole Dihydrochloride (DAPI) staining dyes were purchased from SRL Chemicals (Mumbai).Analytical and HPLC grade reagents Methanol (MeOH) and AR grade DMSO, acetone and Dimethyl Formamide (DMF) were procured from Fischer scientific, India. De-ionized water was used for the

synthesis of NPs and through entire work. All the chemicals were used without any further purification steps.

Human epithelial colorectal adenocarcinoma Caco-2 cells and Human prostate cancer cell lines PC-3 and LNCaP were procured from National Centre for Cell Science (NCCS), Pune (Maharashtra, India). Chemicals for cell culture and cytotoxicity study *viz;* Roswell Park Memorial Institute (RPMI) -1640 media, Dulbecco's modified eagle medium (DMEM), Antibiotic mixture containing penicillin and streptomycin solutions of concentration 1% and Fetal bovine serum (FBS) and other materials used in cell line study were purchased from HI media Laboratories (Mumbai, India). 3-(4, 5-dimethylthiazol-2-yl)-2, 5-diphenyltetrazolium bromide (MTT) were purchased from Sigma Aldrich (St Louis, MO, USA). The blood was collected from a healthy human volunteer from blood bank for carrying out haemolysis study. Molecular biology grade DMSO was purchased from SRL ltd. Annexin V-FITC apoptosis kit was obtained from BD Biosciences. Cell culture flasks, well plates and trans well inserts were purchased from HI media Laboratories. Lucifer yellow dye used in Caco-2 cell permeability study was procured from Thermo Scientific India.

Four months old healthy male Swiss Albino mice (SAM) weighing 22-28g were provided by Zydus Research Centre, Ahmedabad, India for carrying out the pharmacokinetic and biodistribution studies. The experimental protocol was approved by the *Committee for the Purpose of Control and Supervision of Experiments on Animals (CPCSEA) and the Institutional Animal Ethics Committee (IAEC)* having protocol number MSU/IAEC/2017-18/1724. Anticoagulant EDTA disodium salt was procured from Loba Chemie, Mumbai. All the animals were kept under standard laboratory conditions with free access to food and water and acclimatized to the animal facility for at least 7 days before starting the experimental procedures.

6.2.2 Synthesis of bare and functionalised MSNs

The synthesis of bare and surface functionalised MSNs were done as per the procedures described in chapter 5 section 5.2.

6.2.3 ETO loading into mesoporous network

Drug loading was achieved by novel immersion solvent rotary evaporation method (22). Butchi™ Rotary evaporator was used for evaporation of solvent during drug loading. ETO was dissolved completely in methanol in an RBF. Further individual addition of MCM-41, MCM-41-A, PAA-MSN, FA-MSN to the flask in the drug: carrier mass ratio 1:1.5. This was subjected to continuous stirring for 4 h. After this the solvent was evaporated by rotary evaporator and a fine dried powder of ETO loaded MSNs was obtained. The final products were labelled as ETO-MCM-41, ETO-MCM-41-A, ETO-PAA-MSN,ETO-FA-MSN. Drug loading and entrapment were calculated by UV-Vis at 285 nm using the following formulae:

$$Entrapment\ Efficiency = \frac{Total\ weight\ of\ ETO\ present\ in\ nanoparticles}{Weight\ of\ ETE\ added\ initially} \times 100 \ldots . (6.1)$$

$$\%Loading\ Efficiency = \frac{Total\ weight\ of\ drug\ ETO\ present\ in\ nanoparticles}{Total\ weight\ of\ drug\ loaded\ nanoparticles} \times 100 \ldots (6.2)$$

Complete drug loading into the mesopores was confirmed by DSC, FT-IR and WXRD.

6.2.3 In vitro release study:

The drug release pattern was determined and cumulative drug release was calculated for all the mesoporous formulations of ETO. For formulations to be administered by oral route, dissolution study was performed. Additionally simulated and biorelevant media was used to study the effect of enzymes and food on drug release. For parenteral formulations, in vitro diffusion study was performed at different pH values using PBS medium.

6.2.3.1 In vitro dissolution study

Dissolution study was performed using Veego USP type II dissolution apparatus in 900 mL dissolution media at 50 rpm maintaining temperature of dissolution medium at 37 ± 0.5°C. The *in vitro* release study was performed for plain ETO (API), MF, ETO-MCM-41 and ETO-MCM-41-A in acetate media (pH 4.6), simulated gastric fluid (SGF) (pH 1.2) and simulated intestinal fluid (SIF) (pH 6.8) containing pepsin and pancreatin respectively. Enzyme free SGF (pH 1.2) and SIF (pH 6.8) were also taken to study the presence of any interaction between hard gelatin capsule shell and amine group of MCM-41-A and whether it has any effect on the release of ETO. The drug release pattern was also studied in the presence and absence of food as well. Hence, the fed and fasted state simulated gastric and intestinal media were prepared (FaSSGF, FeSSGF. FaSSIF, FeSSIF) for this purpose. The composition of all media is summarized in Table 6.1 (23, 24).The powder was filled in the hard gelatin capsule shell prior to dissolution study. 5 mL aliquots were withdrawn at 5, 10,15,20,30,45,60,90,120,180,240,320 and 360 min intervals. The withdrawn samples were filtered through 0.45µ PVDF filter membrane and analysed by UV spectrophotometer at 285 nm. Sink conditions were maintained throughout the study by adding an equivalent amount of fresh medium as that of withdrawn sample.

Sr No.	COMPOSITION	A	B	C	D	E	F	G	H	I
1	Lecithin	-	-	-	-	-	20μM	-	0.75mM	3.75mM
2	Sodium taurocholate	-	-	-	-	-	80 μM	-	3mM	15mM
3	Pepsin	-	3.2g	-	-	-	0.1g	-	-	-
4	Acetic acid	1.66mL	-	-	-	-	-	2.1g	-	8.65g
5	Sodium acetate	2.99g	-	-	-	-	-	4.01g	-	
6	Sodium chloride	-	2g	2g	-	-	1g	13.85g	3.093 g	11.87g
7	Concentrated Hydrochloric acid	-	7mL	7mL	-	-	-	-	-	-
8	Milk	-	-	-	-	-	-	500mL	-	-
9	Pancreatin	-	-	-	1g	-	-	-	-	-
10	Monobasic potassium phosphate	-	-	-	6.88g	6.88g	-	-	1.977g	-
11	Sodium hydroxide	-	-	-	77mL	77mL	-	-	0.174 g	4.04g
12	pH	4.6	1.2	1.2	6.8	6.8	1.6	1.6	6.5	6.5
13	Deionized Water	Upto 1000mL	Upto 1000 mL	Upto 1000 mL	Upto 1000 mL	Upto 1000 mL	Upto 1000 mL	Upto 1000 mL	Upto 500 mL	Upto 1000 mL

A= Acetate media, B= SGF, C= SGF (Enzyme free), D= SIF, E= SIF (Enzyme free), F = Fast state simulated gastric fluid (FaSSGF), G= Fed state simulated gastric fluid (FeSSGF), H= Fast state simulated intestinal fluid (FaSSIF), I= Fed state simulated intestinal fluid (FeSSIF).

Table 6.1. Composition of various dissolution media used.

6.2.3.2 Dissolution Kinetics study

For the purpose of quantifying the differences in the release profiles of ETO formulations. The drug release data from both MCM-41 and MCM-41-A nanoparticles was fitted to various kinetic models and the best fit was determined. Different parameters by fitting the experimental data to different release models were calculated. Criteria for judgement on best model included lowest AIC (Akaike information criterion), highest MSC (Model selection criterion) and Regression values (R^2) (25). The various release models to which dissolution data were fitted

include zero order, first order, Higuchi, Weibull, Hixon-Crowell and Korsmeyer peppas model (26).

6.2.3.3 In vitro diffusion study

In the *in vitro* drug release study, a suspension of ETO, and ETO-MCM-41, ETO-MCM-41-A, ETO-PAA-MSN and ETO-FA-MSN was filled into a dialysis tube (cutoff Molecular weight (Mw) = 7000 g/mol for PAA-MSNs) and (cut-off Mw=3500 for FA-MSNs). Further, the bag containing filled dispersion was then immersed into 100 mL (Phosphate buffer saline) PBS solution of different pH (5.5, 6.8 and 7.4) with continuous magnetic stirring at room temperature (RT). Sink conditions were maintained by immediate replenishment of the withdrawn samples with fresh PBS. The samples were withdrawn at 2, 4,8,10,12,,24,30,36,48,54,60 and 72h time intervals while maintaining adequate sink conditions to continue the release profile of drug. The samples were filtered through 0.22µm membrane filter prior to analysis. The drug release at particular time intervals was calculated by measuring fluorescence intensity by Spectrofluorophotometer with excitation wavelength fixed at 247 nm and emission measured at 323 nm.

6.2.3.4 Diffusion Kinetics study

The experimental data obtained from diffusion study was fitted to , zero order, first order, higuchi and Korsmeyer peppas kinetic model to determine the release mechanism for ETO. The data was fitted to appropriate model to determine the n value and in turn the release mechanism. DD-solver; an excel-add in was used for this purpose.

6.2.4 In vitro cytotoxicity study

Three different cell lines were used in the entire study. Caco-2 cells were used in determination of permeability in case of oral formulation. Whereas, two prostate cancer cell lines androgen independent PC-3 and androgen dependent LNCaP were used to determine the efficacy of the parenteral formulations.

6.2.4.1 Caco-2 cell line

For the purpose of studying cytotoxicity of ETO, ETO-MCM-41 and ETO-MCM-41-A MSNs. MTT assay was carried out on Caco-2 cells. Caco-2 cells were cultured at low passage number. The cells were maintained at 37°C in an incubator and 5% Carbon dioxide supply in DMEM medium supplemented with 20%FBS and 1% Pen-strep solution to aid in avoiding any sort of contamination. The cells were seeded at a density of 10,000 cells per well in complete DMEM media in 96 well microtiter plates. This was followed by nanoparticle treatment for 24 and 72h in a fresh incomplete DMEM medium in concentration range 0.1-100 µg/mL. Next, 100 µL MTT dye was added to each well and incubated for 4 h. Ultimately, 100 µL DMSO was added to solubilize the formazan formed. After 10 min the plates were read at 590 nm using plate reader, % cell viability was calculated as per the formula given below where O.D. stands for optical density. Blank was devoid of any cells.

$$\%Cell\ Viability = \frac{O.D._{\cdot sample} - O.D._{\cdot blank}}{O.D._{\cdot negative\ control} - O.D._{\cdot blank}} \times 100 \ldots\ldots\ldots (6.3)$$

6.2.4.2 LNCaP and PC-3 cell lines

Human prostate cancer cell lines PC-3 and LNCaP were used to evaluate the cytotoxicity of MCM-41, MCM-41-A, ETO-MCM-41, ETO-MCM-41-A, ETO-MCM-41-A, PAA-MSN, ETO-PAA-MSN, FA-MSN, ETO-FA-MSN and free ETO by colorimetry based 3-(4,5-dimethylthiazol-2-yl)-2,5-diphenyltetrazolium bromide (MTT) assay. The cells were cultured at low passage. The media used was RPMI-1640 supplemented with 10 % Foetal Bovine serum FBS and 1 % antibiotics (Pen-Strep). The cell line was regularly screened and confirmed for absence of any sort of contamination. Cells were maintained in a humified, 5% CO_2 tissue culture incubator at 37 °C.

Cancer cells were seeded in 96-well microtiter plates at a density of 9,000 cells per well in complete RPMI-1640 media supplemented with 10% FBS. After 24, 48 and 72 h cells were

incubated with fresh RPMI-1640 containing ETO, (0.1-20 and 2-60 µg/mL); known amount of ETO loaded NPs corresponding to the aforementioned range. For adjudging the carrier toxicity; PAA-MSNs and FA-MSNs were incubated with cells for 72h in the concentration range of 0.1 to 100 µg/mL. All the dilutions were done in RPMI-1640 media. Furthermore, on next day MTT treatment was given to cells with 100µL dye added to each well and again incubated for 4 h. This was followed by addition of 100 µL DMSO to solubilize the formazan formed. The difference in intensity of purple color obtained in wells was analyzed by Plate reader at 590nm. Finally, cell viability was determined by the following equation

$$Cell\ viability\ (\%) = \frac{I\ (sample) - I\ (blank)}{I\ (control) - I\ (blank)} \ldots\ldots (6.4)$$

Where I sample, I control and I blank represents absorbance intensity at 590 nm, for cells treated with different samples (Positive control), for Negative control cells (untreated cells+ MTT+ DMSO), and blank well devoid of cells (Media + MTT + DMSO) respectively.

6.2.5 Caco-2 monolayer cell line permeability study:

Caco-2 cell line was maintained at 5% Carbon dioxide, 37°C and complete RPMI-1640 with 20% FBS and 1% antibiotics (Pen-Strep solution). The Caco-2 cells were grown on trans well inserts having 0.4µ pore diameter with 1.13 cm^2 area. The inserts were thoroughly washed with 25mM HBSS Hank's balanced salt solution of 7.4 pH. The integrity of the monolayer formed was tested by monitoring Lucifer yellow dye permeability across the layer. Time dependent transport of ETO loaded MSNs was studied in unidirectional apical to basal manner. The donor compartment (apical) was treated with 0.5 mL of transport solution i.e. HBSS containing 0.1 mg/mL ETO and basal side was treated with 1.5 mL of HBSS solution. The samples were analysed by HPLC equipped with fluorescence detector with excitation wavelength of 247 and emission measured at 323nm.

After incubation of 30, 60, 90, 120, 180, 240 and 300 min, 100µL aliquots were withdrawn from the receiver and replenished with same volume of fresh HBSS. The collected samples were further analysed by HPLC equipped with fluorescence detector. The apparent permeability coefficient (Papp) was measured using the following equation. $Papp = dQ/dt/A \times C_0 * 60$ ……...(6.5)

Where,

Papp: Apparent permeability coefficient (cm/h)

dQ/dt: drug permeation rate (mg/min)

A: cross-sectional area *i.e.* 1.13 cm^2

C_0: Initial drug concentration in the donor compartment (mg/mL)

6.2.6 In vitro cellular uptake study

5.2.6.1 Intracellular qualitative uptake study by confocal microscopy

LNCaP and PC-3 cells were seeded on a coverslip in 6 well plates and grown in a complete RPMI-1640 medium. Thereafter, the cells were exposed to FITC#MCM-41-A, FITC#PAA-MSNs, FITC#FA-MSN and Free FA+FITC#FA-MSN for 12 and 48 h. The medium was removed and then washed thrice with PBS. Later, the coverslips were washed thoroughly with the PBS and fixed with 3% paraformaldehyde (27). Lastly, LNCaP and PC-3 cells on coverslips were counter stained with DAPI (nuclear stain) in PBS (1µg/ml) at RT for 30 min and images were taken on a confocal microscope.

6.2.6.2 Intracellular quantitative uptake study by Flow cytometry(FACS or FCM)

The cellular uptake was determined by Flow cytometry. PC-3 and LNCaP cells were seeded in a 12-well plate at density of 1×10^6 cells per well and incubated for 24h. Untreated cells were taken as control. Both the cells were treated with FITC#MCM-41-A, FITC#PAA-MSN, FITC#FA-MSN and Free FA+FITC#FA-MSN. After appropriate incubation time of 48 h medium was completely removed and cells were washed with PBS two times followed by

trypsinization. Here, all the free FITC-MSNs and dead cells were removed. All the cells were collected and centrifuged at a speed of 1200rpm and washed with PBS. This was again followed by resuspending in PBS. The cell suspensions were filtered through cell strainer and further subjected to flow cytometric analysis (FACS Calibur).

6.2.7 Evaluation of cell death mechanisms by apoptosis assay

Annexin V-FITC double stain apoptosis detection kit from BD Biosciences was used for determining percentage of apoptotic and necrotic cells by standard Fluorescence activated cells sorting (FACS) assay. LNCaP and PC-3 cells were seeded each at a density of 10^6 cells per well and incubated for 24 h. The cells were treated with ETO solution, ETO-MCM-41-A, ETO-PAA-MSN and ETO-FA-MSN and incubated for 24 h followed by cold PBS (4℃) wash. Untreated cells were taken as control. The washed cells were then stained using FITC-Annexin V apoptosis detection kit. Concisely, the cells were suspended in 1 mL of 1 × binding buffer at a concentration of 1×10^6 cells/mL. Further, 5µL of FITC-Annexin V and 5µL of PI were added per 100µL of the suspension (1×10^5). After mild vertexing, the cells were incubated for 15 min in dark. Finally, 400 µL of 1 × binding buffer was added to each tube and analysed by FCM (28).

6.2.8 Haemolysis study

Haemolysis study was performed to investigate if the prepared MSNs caused any lysis of the RBCs. Herein, both qualitative and quantitative hemocompatibility study was performed by microscopy and UV-Vis spectrophotometry respectively. Erythrocytes treated with Triton X100 were taken as a positive control; where maximum amount of haemolysis was observed. Erythrocytes in PBS 7.4 were taken as negative control, wherein, almost no lysis was observed. Positive control, negative control and ETO-MCM-41, ETO-MCM-41-A and ETO-PAA-MSN and ETO-FA-MSN were incubated with erythrocytes and images were taken post incubation. Thereafter UV-Vis quantitative analysis of supernatant was performed after centrifugation.

6.2.9 In vivo pharmacokinetic study

6.2.9.1 Pharmacokinetic study for oral formulation

6.2.9.1.1 Experimental:

To study the oral bioavailability, mice were assigned into 5 groups including control. Group -I was administered 0.9% NaCl saline solution and labelled as control group (negative control). Group -II animals were administered ETO suspension dose equivalent to 10mg/kg. Group III, IV, V were administered ETO-MCM-41. ETO-MCM-41-A and ETO Marketed formulation (MF) all dose equivalent to 10mg/kg ETO respectively. All the formulations were administered by direct introduction into stomach using oral gavage. The blood samples were withdrawn using a capillary tube at 0.5, 1,2,4,6,24 h post dosing from the retro orbital venous plexus and collected in EDTA treated tubes.

6.2.9.1.2 Sample preparation:

Protein precipitation method was employed for extraction of sample from the biological matrix. Further, plasma was separated from the collected samples by centrifugation at 4000 rpm for 10 minutes at 4℃. 100µL plasma was mixed with internal standard (10 µL, 5ppm) Tapentadol (TAP). The samples were precipitated by adding 300 µL Methanol (MeOH) and again centrifuged at 10000 rpm for 10 min. The supernatants were collected and ETO was quantified using a HPLC equipped with a fluorescence detector. The parameters of HPLC method developed were ammonium formate (20mM) and methanol in the ratio 49:51 on a waters symmetry 300 C-18 column (250mm× 4.6mm×5µ) at pH 3.9 with a flow rate of 1mL/min. Pharmacokinetic parameters were calculated using excel add-in pk solver.

6.2.9.1.3 Pharmacokinetic parameters evaluation

Different pharmacokinetic parameters were calculated from the plasma concentration time data by means of a model independent method *i.e.* non-compartmental module using PK solver excel add-in. Peak plasma concentration (C_{max}), $T_{1/2}$ and time required for achieve C_{max} *i.e.* t_{max}

were obtained by visual inspection of the experimental data. Moreover, the linear trapezoidal method was applied to determine area under curve (AUC_{0-t}).

6.2.9.2 Pharmacokinetic study for parenteral formulation

For pharmacokinetic study mice were randomly divided into 5 groups and intravenously injected from the tail vein with a 0.5 CC U40 insulin syringe fitted with a 28-$g^{1/2}$ needle. Group-I was assigned as a control group with no drug administered. Group II,III,IV and V were administered with 200µL of sterile suspension of free ETO, ETO-MCM-41-A, ETO-PAA-MSN and ETO-FA-MSN (10 mg/kg) body weight respectively. The blood samples (0.3 ml) were collected at specific time intervals of 0.25, 0.5, 1.2, 4.6.8 and 12 h and stored in EDTA containing centrifuge vials. Further, plasma was separated by centrifugation at 4000 rpm for 10 minutes at 4°C. 100µL plasma was mixed with internal standard TAP. The samples were precipitated by adding MeOH and again centrifuged at 10000 rpm for 10 min. The supernatants were collected and ETO was quantified using a HPLC equipped with a fluorescence detector. The parameters of HPLC method developed were ammonium formate (20mM) and methanol in the ratio 49:51 on a waters symmetry 300 C-18 column (250mm× 4.6mm×5µ) at pH 3.9 with a flow rate of 1mL/min. Pharmacokinetic parameters viz C_{max}, T_{max} and AUC were calculated using excel add-in pk solver.

6.2.9.3 In vivo biodistribution study and histological examination

For studying biodistribution of ETO and MSNs, in major organs, mice were assigned into 4 groups (n=3) including control, free ETO, ETO-MCM-41-A,ETO-PAA-MSN and ETO-FA-MSN. The experimental groups were administered sterile ETO suspensions and NP suspensions at dose of 10 mg/kg. Sterile saline injections (0.9% NaCl) at equivalent volumes were given to mice as control. Mice were sacrificed at 24 h after injection and major tissues like heart, liver, lung, kidney, brain and spleen were collected and weighed. Furthermore, PBS solution was added to each tissue sample by an equal volume to its weight and subjected to

high speed homogenization. The mixtures obtained were centrifuged at 10000 rpm for 10 min. The supernatant was collected and extracted with MeOH. The obtained solution was transferred to centrifuge vials and subjected to evaporation. The dried residues were reconstituted in 100µL MeOH. The amount of ETO in each tissue was quantified by HPLC equipped with a fluorescence detector with excitation at 247 and emission at 323 nm.

The major organs collected were fixed in 10 % formalin solution. The organs were embedded in paraffin and sectioned to 4um sections and placed onto the glass slides. The histological sections were stained with Haematoxylin and Eosin stain (H&E) and observed under microscope. This was performed to determine the *in vivo* toxicity of various ETE formulations.

6.2.10 Statistical analysis

The experiments were conducted thrice, and the results were expressed as the means and standard deviations from the triplicate experiments unless mentioned otherwise. The statistical analysis was performed by one-way ANOVA and p-values less than 0.05 were considered as significant.

6.2.11 Stability study of mesoporous silica nanoparticles

The stability study of synthesized MSNs i.e. ETO-MCM-41, ETO-MCM-41-A, ETO-PAA-MSN, and ETO-FA-MSN was performed as specified in ICH Q1A(R2). The synthesized nanoparticles were exposed to 40±2 ºC and 75±5 %RH conditions and sampling was done at 0^{th} day, 3^{rd} month and 6^{th} month and samples were analysed by DSC and LXRD.

6.3 Results and discussion

6.3.1 Solid state evaluation

6.3.1.1 Fourier Transform-Infra Red (FT-IR) spectroscopy studies

FT-IR is useful in qualitative estimation for identification of functional groups present. In FT-IR spectra of ETO (Fig 6.1 (a)) showed several characteristic bands. The band corresponding to C-H stretch was observed at 2950 cm^{-1}. C=O stretch for ester and carboxy methyl was

obtained at 1752 and 1610 cm-1 respectively. The C-O-C stretch was observed with bands observed at 1034 cm^{-1}. Bands obtained at 1478 and 1426 cm^{-1} could be attributed to the C=C stretching in the backbone of the aromatic phenyl ring.

All the MSN spectra exhibited bands that are characteristic of mesoporous silica (Fig 6.1). In FT-IR spectra of MCM-41, the typical bands at 811cm and 1085 cm^{-1} could be attributed to bending and asymmetric stretching of Si-O bonds. The vibrational band at 965 cm^{-1} is a characteristic feature of Si-OH group routinely observed in silica material. The broad band pivoted at 3439 cm^{-1} is attributed to the hydroxyl stretching (O-H) due to the silanol groups. Large number of CTAB present in asynthesized MSNs gave typical C-H stretching vibrations at 2954 and 2898 cm^{-1} and C-H deformation vibration at 1452 cm^{-1}. However, after evacuation of CTAB all the bands occurring due to presence of surfactant disappeared. Newer bands in the spectra of MCM-41-A stipulate the successful incorporation of the amine groups via functionalization. During surface decoration of MCM-41, the hydroxyl groups present on the surface of mesoporous silica react with APTES resulting in formation of Si-O-Si bonds. The reduction in hydroxyl group is an evidence of anchoring mechanism being involved in the reaction between silanol groups and APTES (29). A new band allocated to asymmetric bending of $-NH_2$ was observed at 1590 cm^{-1}. Moreover, a couple of bands assigned to CH_2 stretching were obtained at 2870 and 2930 cm^{-1}. Additionally, the prominent NH stretching mode can be observed at 3340 cm^{-1}. Moreover, there was a decrease in intensity of Si-O-Si stretching band at 1085 cm-1 in case of MCM-41-A, indicating lowered amount of free silanol groups caused by attachment of NH_2 groups to the surface of silica. The existence of these peaks, altogether confirm the success of functionalization strategy. Successful functionalization with PAA was confirmed by new adsorption peaks appearing at 1551, 1650 and 1714 cm-1 assigned to N-H bending, C=O stretching vibration in amide group and C=O stretching vibration in carboxyl group respectively.

New Bands appeared in the spectra of FA-MSN (Fig 6.1(i)). It is a clear indication of successful incorporation of organic groups onto MCM-41. Weak band at 2832 cm^{-1} is attributed to vibrational C-H of CH_2 groups present in FA. Peak at 1511 cm^{-1} corresponds to aromatic ring vibrations of C=C of FA. The newer band at 1609 cm^{-1} is belongs to typical C=O vibration. The N-H stretching band at 3346 cm^{-1} is superposed to vibrational O-H band. The superposed bands at 1606-1539 cm^{-1} could be assigned to stretching C=N, bending N-H and O-H vibrations. These results indicated a successful grafting of FA ligand on MCM-41 surface which is in sync with the results of elemental analysis.

The drug loaded FT-IR spectra of both MSNs exhibited completely resolved peak of mesoporous silica. Additionally, most of the characteristic peaks of the drug are either not well visible or completely disappeared, due to fine housing of drug into MSN pores rather than on the surface. A similar pattern was obtained in ETO loaded MSNs. This could be attributed to a complete encapsulation of ETO into the silica pores.

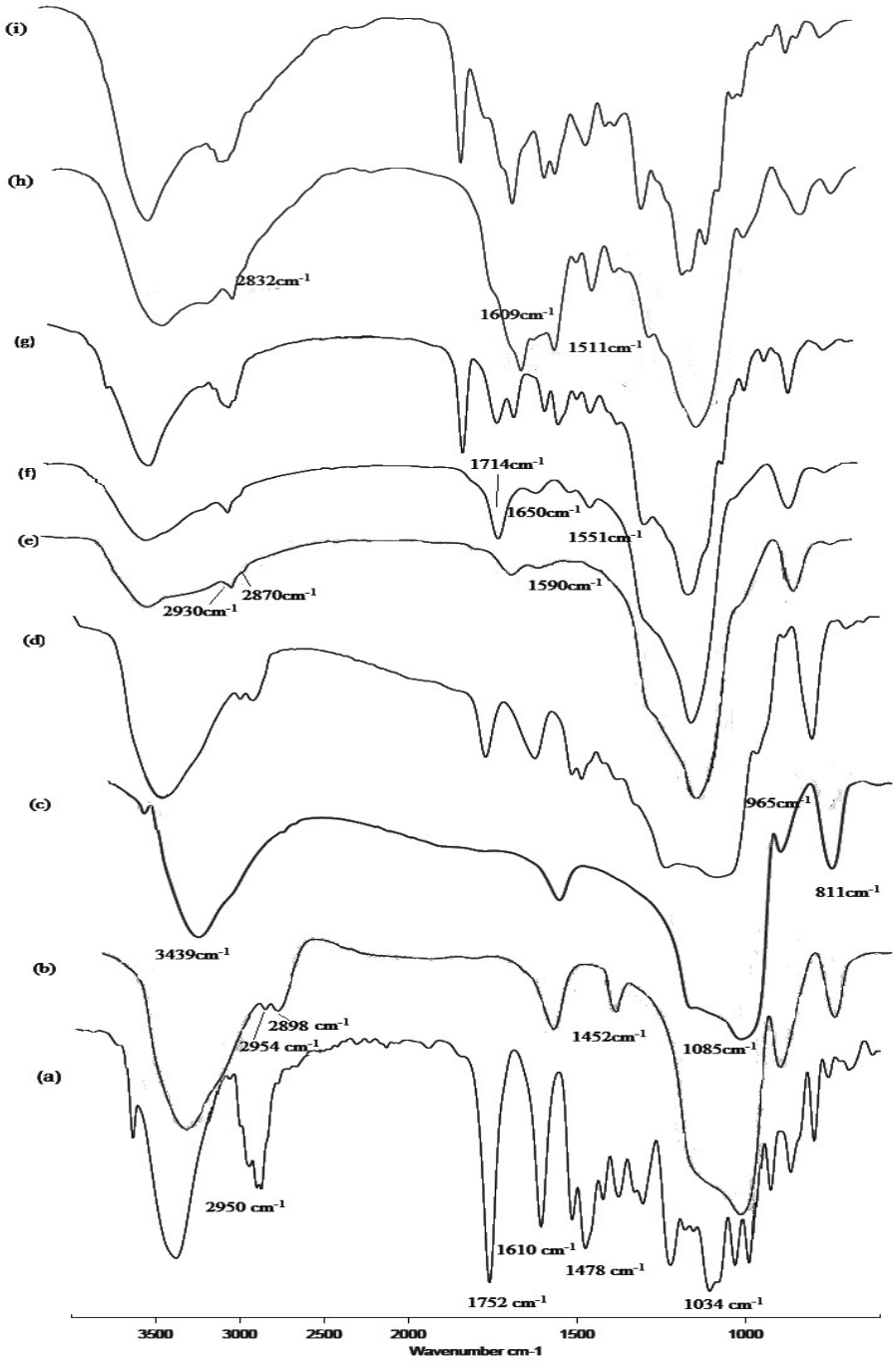

Figure 6.1. FT-IR Spectra (a) ETO (b) Asynthesised MSN (c) MCM-41 (d) ETO-MCM-41 (e) MCM-41-A (f) PAA-MSN (g) ETO-PAA-MSN (h)FA-MSN (i) ETO-FA-MSN

6.3.1.2 Differential scanning calorimetry (DSC) analysis

The existence of ETO on silica matrix in amorphous or crystalline form and complete encapsulation was further confirmed by DSC. The DSC curve of ETO showed a solitary

endothermic peak at 281.83°C (Fig 6.2 (a)), owing to its intrinsic melting point. If the drug is present in the crystalline form in the mesopores, the quantity of drug can be differentiated and calculated from the melting point depression by DSC. Absence of any melting point depression is indicative of presence of drug in non-crystalline state in pores (30). Thermograms of all ETO loaded MSNs were recorded and signals due to melting were noted. Notably, no endothermic transition was observed in thermogram corresponding to the ETO: MCM-41 mass ratio of 1:1.5. and similar for ETO-MCM-41-A, ETO-PAA-MSN and ETO-FA-MSN as well.

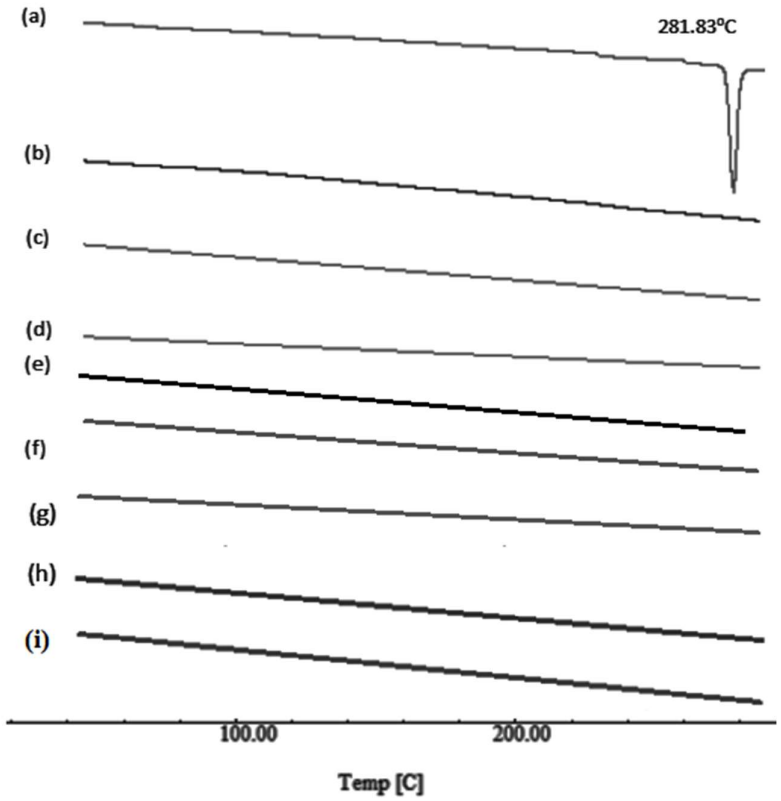

Figure 6.2. DSC thermograms of (a) Crystalline ETO (melting point of drug), (b) MCM-41 (c) ETO-MCM-41, (d) MCM-41-A (e) ETO-MCM-41-A (f) PAA-MSN (g) ETO-PAA-MSN (h) FA-MSN (i) ETO-FA-MSN

6.3.1.3 Thermogravimetric analysis

The thermogravimetric analysis was used to deduce the extent of functionalization and quantity of drug entrapped in the mesoporous material. It is recorded as a temperature dependent weight

reduction (29). TGA curves are shown in (Fig 6.3).The unmodified MCM-41 showed two easily distinguishable weight loss regions. The first region of weight loss occurs in a temperature range of 20- 150°C. This could be accredited to the thermodesorption of physically adsorbed water from the surface of silica. The following second region of temperature range (150-650°C), the TGA curve is comparatively flat and weight loss is slender. This could be imputed to the silanol condensation (31). All the MSNs exhibited excellent stability within the studied temperature range.

The TGA curves of the functionalized MCM-41-A are somewhat different than that of their unmodified counterpart (MCM-41). The samples which show a decreased value of weight loss in the first characteristic region are indicative of an increasing hydrophobic character of a material and overall decrease in the silanol concentration (32). The weight loss between the 150 and 700 °C indicates decomposition of the grafted organic material (Coating or ETO). Increased percentage weight loss is indicative of higher grafting of amino groups or higher loading of ETO. The quantity of amino groups grafted in MCM-41-A is about 4.0 weight percent.

The curves on commencement in case of aminated, PAA and FA functionalized MSNs exhibited a comparative decreased weight loss which may be attributed to the reduction in silanol groups post surface functionalization. Other thermograms obtained served as a reliable proof that ETO was completely encased inside mesopores of bare and functionalized MSNs, as no peak attributed to ETO was visible.

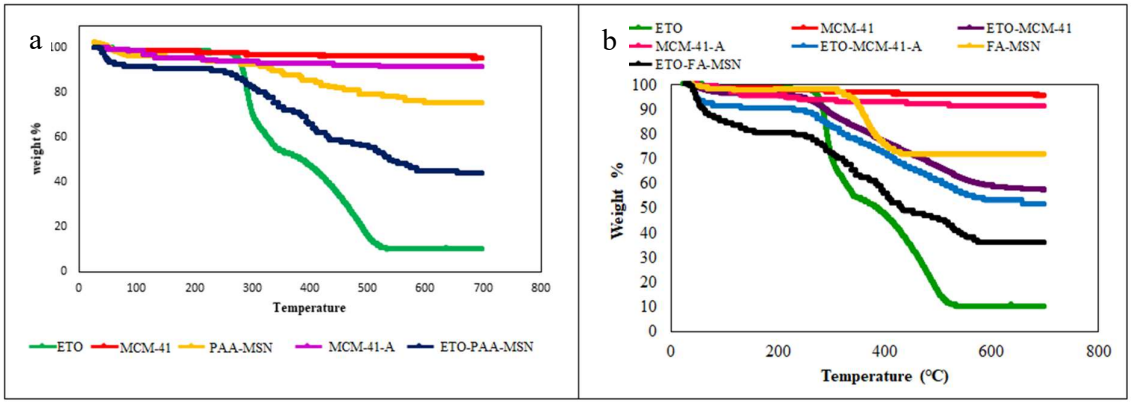

Figure 6.3. (a)& (b) TGA data for developed bare and functionalized mesoporous formulations including the drug loaded MSNs.

6.3.1.4 Wide angle X-Ray diffraction analysis (W-XRD)

The crystalline nature of etoposide was confirmed by wide angle XRD spectra (Fig 6.4(a)). Six characteristic sharp and intense peaks were obtained at 10.9◦, 16.5◦, 19.9◦, 21.3◦, 24.1 and 25.9◦. Wide angle XRD patterns were registered to investigate if the crystalline phase of ETO could be detected. Nevertheless, no crystalline ETO was detected in ETO-MCM-41 and ETO-MCM-41-A, ETO-PAA-MSN and ETO-FA-MSN (Mass ratio 1:1.5). Absence of any characteristic peak in loaded carrier is indicative of the fact that ETO loaded into the MSNs was in a non-crystalline state. Also, the XRD pattern obtained for MCM-41, MCM-41-A, PAA-MSN and FA-MSN NPs was amorphous. The obtained XRD results augmented those obtained from thermal analysis.

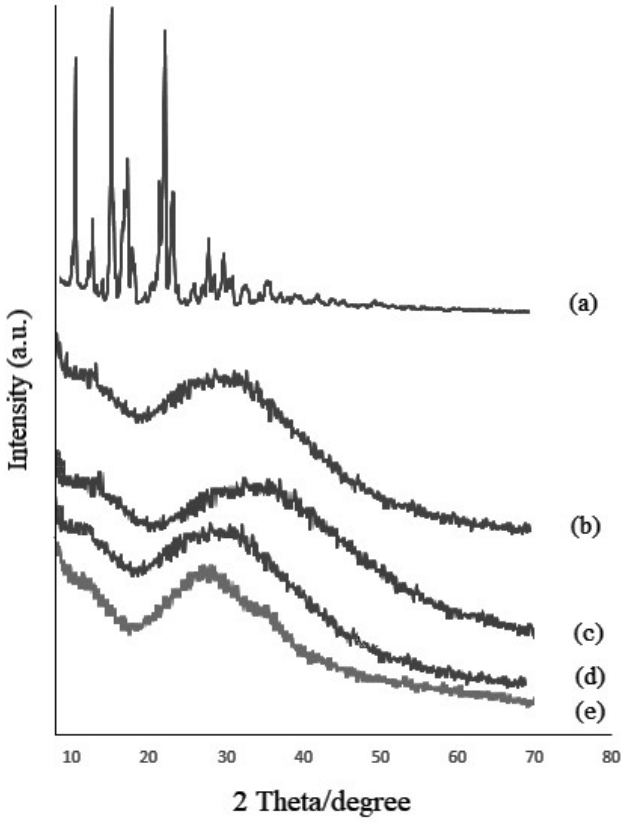

Figure 6.4. WAXRD spectra (a) ETO (b) ETO-MCM-41 (c) ETO-MCM-41-A (d) ETO-PAA-MSN (e) ETO-FA-MSN

6.3.1.5 Low angle X-Ray diffraction

The structure of pores was ascertained by small-angle XRD measurements. The LXRD pattern of pure and functionalized MSNs is depicted in Fig 6.5 (a) – (h). The XRD pattern of MCM-41, MCM-41-A, PAA-MSN and FA-MSN depicted well resolved diffraction peaks characteristic of well-ordered hexagonal arrays of MCM-41 NPs (33). Prominent reflection at 100 and well resolved couple of other reflections 110 and 200 at 2 theta 2.0, 3.6 and 4.3 respectively, characteristic of hexagonal structure of MCM-41. Thus, it can be inferred that the original structure remained intact and there was no loss of structural ordering post functionalization and loading. Though there was a slight decrease in intensity of the characteristic peaks and minor shift towards the right, the mesostructured of the host is still

intact with mesostructured characteristics as identified from the characteristic peaks still visible post functionalization (34).

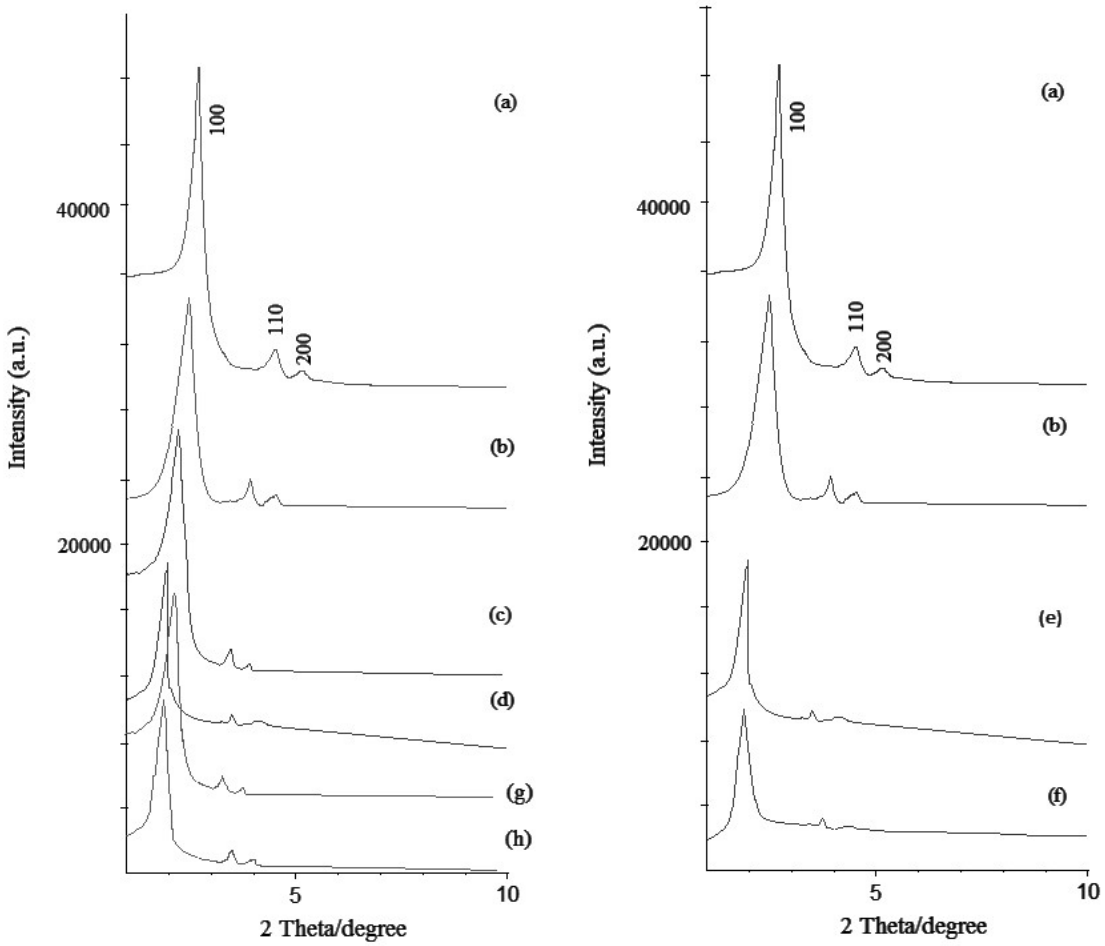

Figure 6.5. LXRD Spectra (a) MCM-41 (b) ETO-MCM-41 (c) MCM-41-A (d) ETO-MCM-41-A (e) PAA-MSN (f) ETO-PAA-MSN (g) FA-MSN (h)ETO-FA-MSN

6.3.1.6 Zeta potential and size determination:

Zeta potential indicates the surface residual charge of the particles. The zeta potential values of MCM-41 was found to be -36.86 mV. This can be attributed to the large number of silanol groups on silica surface (35). Post functionalization with positively charged amino groups, zeta potential changed to +33.92 mV. Loading of ETO into both MCM-41 and MCM-41-A gave zeta potential values of -37.25 and +29.40 mV respectively. However, loading of ETO

did not alter the nature of surface charges in either case. The z average diameter was found to be around 110.2 nm for MCM-41 NPs and 124.7 nm for MCM-41-A NPs, as depicted in the graphs (Fig 6.6). The zeta potential values for ETO-MCM-41, ETO-MCM-41-A and ETO-FA-MSN were -37.25, 29.4 and 41.27mV respectively. Z average diameter for MCM-41 and MCM-41-A was found to be 110.2 nm, 124.7 nm respectively (Fig. 6.6). After functionalization with PAA, the value dropped to -31.15 mV due to the occurrence of large number of acidic carboxylic groups in polyacrylic acid. PAA decorated MSNs exhibited Z average diameter of 142.85 nm. FA-MSN exhibited z average diameter of 135.38 nm. There was an evident increase in size with surface coating. All values are mentioned in table 6.2.

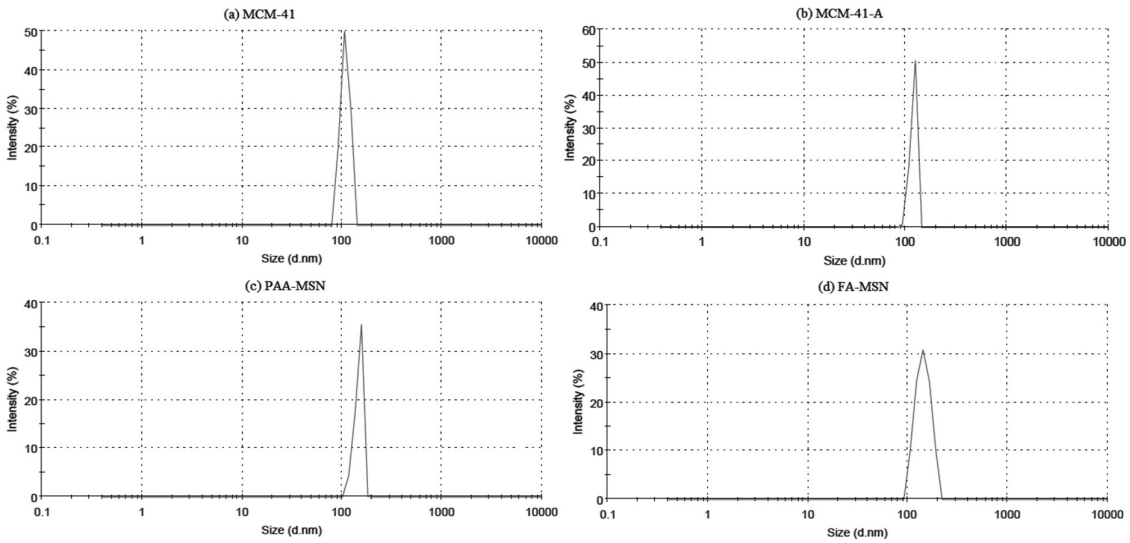

Figure 6.6. Size distribution by intensity (a) MCM-41 (Z average 110.2 nm) and PDI 0.34 (b) MCM-41-A (Z average 124.7 nm) and PDI 0.28 (c) PAA-MSN (Z average 142.85 nm) and PDI 0.39 (d) FA-MSN (Z-average 135.38 nm) PDI 0.42

Sr no	SAMPLE	HYDRODYNAMIC SIZE (nm)	ZETA POTENTIAL (mV)s
1	MCM-41	110.2	-36.86
2	ETO-MCM-41	-	-37.25
3	MCM-41-A	124.7	+33.92
4	ETO-MCM-41-A	-	+29.40
5	PAA-MSN	142.85	-31.15
6	ETO-PAA-MSN	-	-39.42
7	FA-MSN	135.38	+36.04
8	ETO-FA-MSN	-	+41.27

Table 6.2. Zeta potential and size data for bare, surface functionalized and drug loaded MSNs

6.3.1.7 Nitrogen sorption analysis:

N_2 adsorption was used to determine pore size distribution, pore volume and BET surface area. The values obtained from Isotherms (Fig 6.7) are listed in Table 6.3 . Bare MCM-41 shows type 4 isotherm, with infliction observed at p/po ratio of about 0.8, which is a characteristic property of mesoporous materials having a large surface area and narrow pore size distribution (36). Both the nanoparticles MCM-41 and MCM-41-A possessed a large surface, which justifies their potential application as hosts for storing more drug molecules for drug delivery purpose (37).

The N_2 desorption curve showed hysteresis which confirmed the mesoporous structure. The characteristic trait of type IV isotherm is its hysteresis loop and mesoporous materials having monolayer-multilayer adsorption with a capillary condensation tend to generate this kind of hysteresis loop attributed to difference between adsorption and desorption (36). The mesoporous characteristics of MSNs remained intact and well preserved after loading as seen from the N_2 adsorption isotherm post loading of ETO. The bare silica (MCM-41) Isotherm depicts sharp increase in N_2 adsorption at $0.2< P/Po<0.3$. As inferred from values in table 6.3 functionalized silica showed a decrease in surface area and pore volume. This relation was directly proportional. This decrease supports the fact that the wall of pores is covered by organic

moieties. There was also decrease in the pore diameter as functionalization proceeded from unmodified silica to MCM-41-A.Predictably, post functionalization there was decrease in surface area and pore volume due to instigation of organic moiety. Although there was decrease in surface area with functionalization, the final PAA-MSNs and FA-MSNs had sufficiently large area to serve as hosts to entrap drug molecules in sufficient amount for excellent drug delivery applications. The mesoporous characteristics were well preserved post ETO loading in all the nanocarriers as depicted from the isotherms obtained.

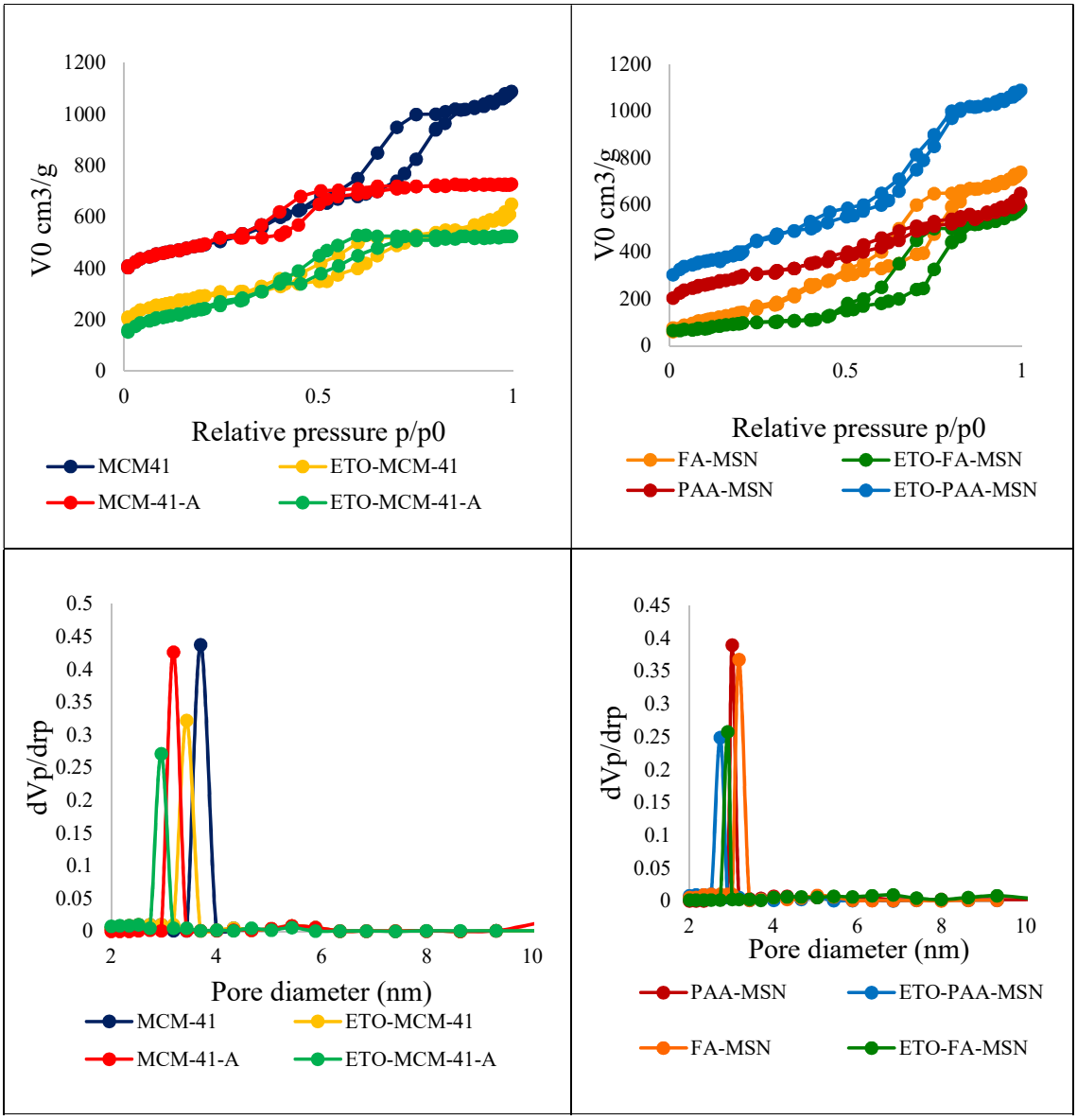

Figure 6.7. Surface area and pore size distribution of the MSN

Sr No	Parameters	MCM-41	MCM-41-A	ETO-MCM-41	ETO-MCM-41-A	PAA-MSN	ETO-PAA-MSN	FA-MSN	ETO-FA-MSN
1	BET Surface (m^2/g)	1089.97	827.90	850.74	624.79	702.84	565.87	745.72	520.16
2	BJH (surface area (m^2/g)	1441.97	1165.49	977.23	780.21	878.34	689.92	921.87	610.33
3	Pore size (nm)	3.69	3.43	3.42	3.18	3.02	2.73	3.22	2.91
4	Pore volume (cm^3/g)	0.4377	0.4261	0.3218	0.2710	0.3895	0.2489	0.3672	0.2573

Table 6.3. Porosity and surface properties of MSNs

6.3.1.8 SEM and TEM analysis:

SEM images of MSNs are shown in Fig 6.8 . The SEM micrographs divulge spherical morphology of synthesized particles MCM-41 NPs. There are certain limitations associated with SEM in giving a detailed in depth structure of the nanoparticle. Hence, additionally TEM analysis was also performed to ascertain the porous structure of MSN. Clear well defined Honey comb like hexagonal network was visible in the TEM images (Fig 6.9). MCM-41 TEM images were evidence that clear mesostructures were present in the samples and were still intact. PA-MSNs and FA-MSNs were seen to be well ordered with honeycomb like structure evident of well-preserved mesoporous characteristics post functionalization.

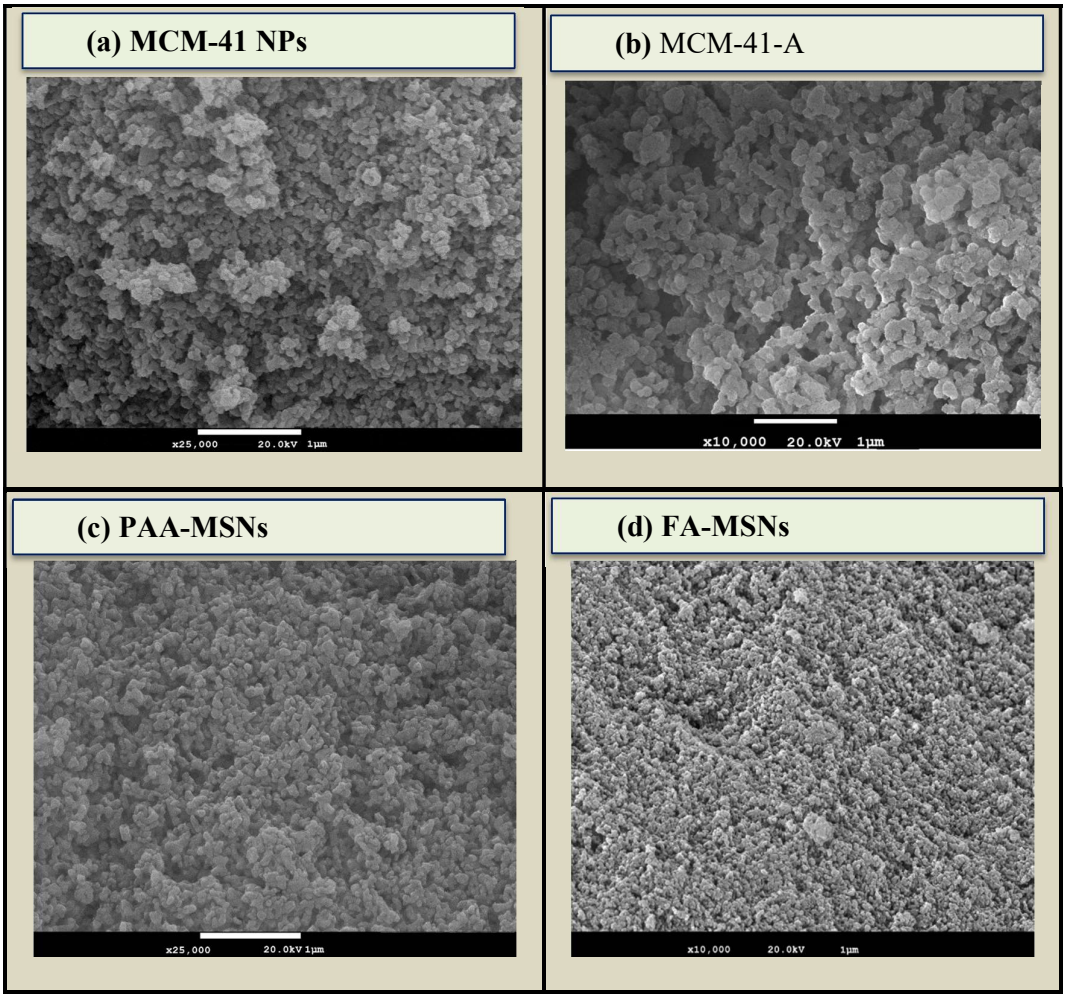

Figure 6.8. SEM images of MSNs (MCM-41 and surface functionalised MSNs viz, MCM-41-A, PAA-MSN, FA-MSN)

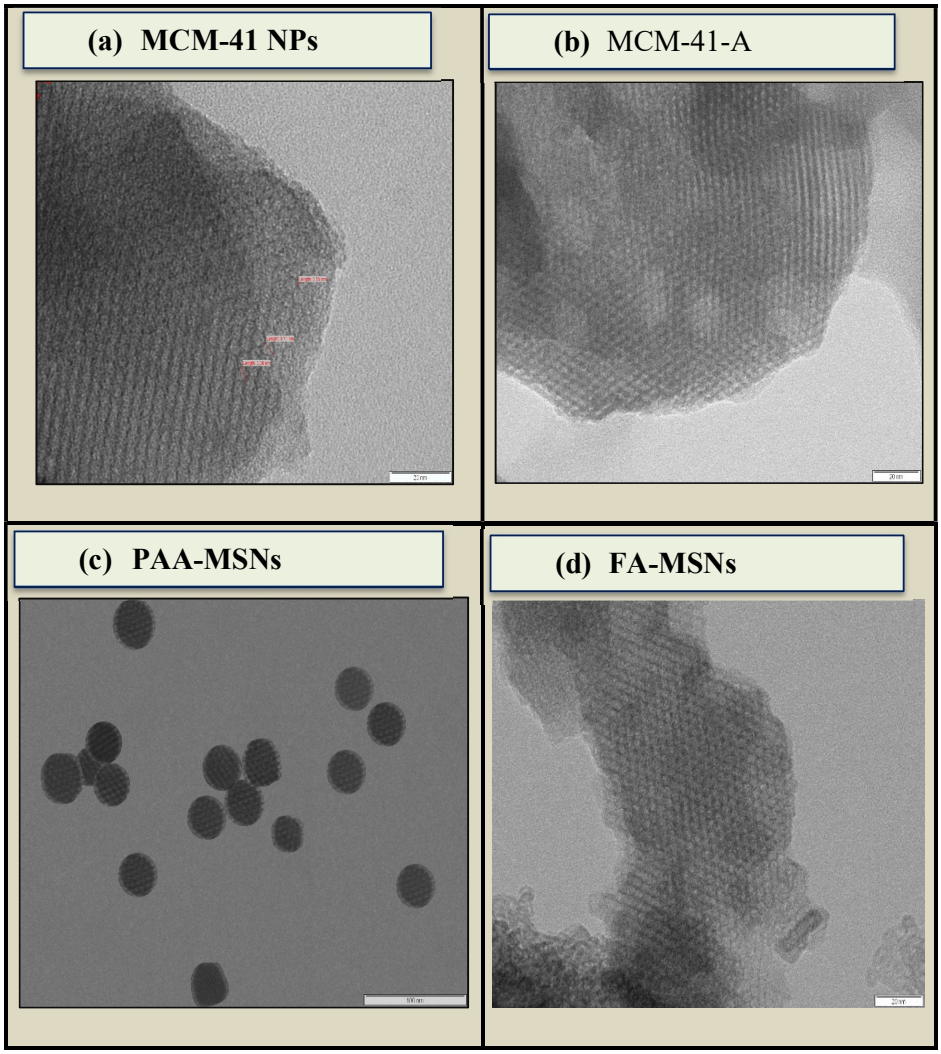

Figure 6.9. TEM images of MSNs (MCM-41 and surface functionalised MSNs viz, MCM-41-A, PAA-MSN, FA-MSN)

6.3.1.9 Elemental detection and quantification of surface moiety

There was wide difference in the elemental composition of all the three MSNs as expected(Figure 6.10). In case of MCM-41 (bare silica) elemental composition of Si (37.9%) and O (62.1%) was observed. However, post amination the composition changed to Si (29.3%), O (40.3%), C (27.6%) and Nitrogen (2.8%). There was introduction of Carbon and Nitrogen

after amination. Further, EDS spectra of PAA-MSN revealed (C 47.6%), O (34.2%), Si (18.2%) and absence of N. Thus, this further confirmed that complete functionalization with high grafting % of PAA was achieved. This is attributed to the fact that there was tremendous increase in C percentage and no Nitrogen was detected in case of PAA-MSN.FA groups were responsible for further increase in % of C and N. Folic acid grafting is supported by increase in N and C content and decrease in the O percentage. A successful grafting can be concluded by the promising quantitative results.

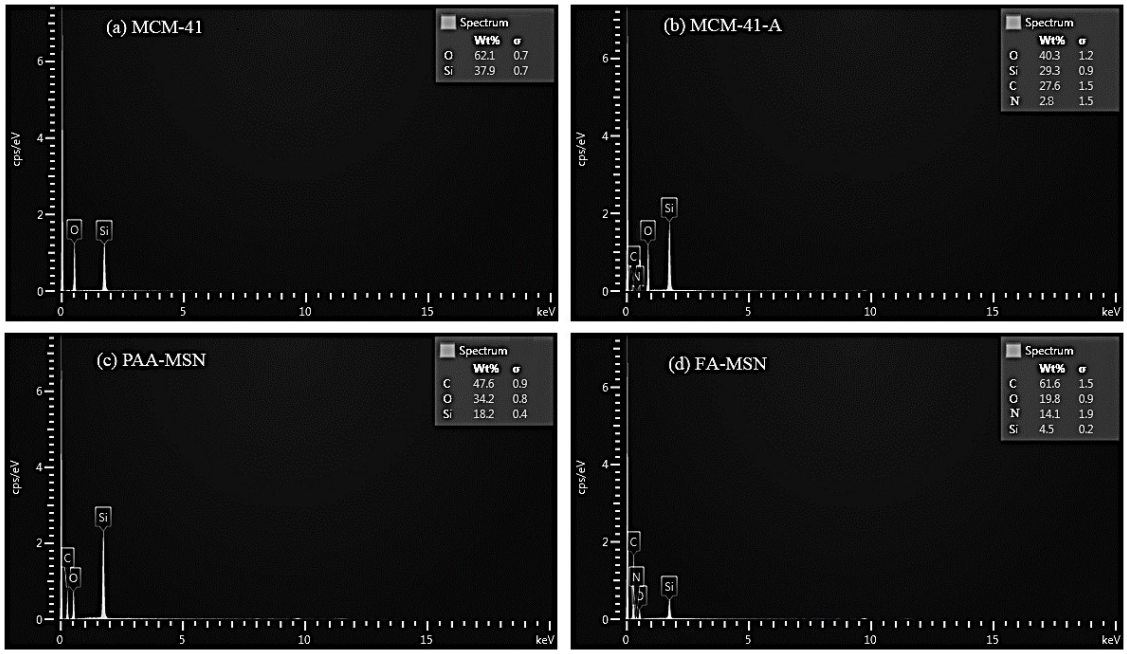

Figure 6.10. SEM-EDS images of (a) MCM-41 (b) MCM-41-A (c) PAA-MSNs (d) FA-MSNs

6.3.2 Estimation of drug loading efficiency

The pore size and pore volume also contribute in determining the maximum amount of drug which can be entrapped in MSNs. A slight reduction in loading percentage from MCM-41 to post functionalization in MCM-41-A was observed. Additionally, the TGA data also prove the thermal stability of silica materials for proposed potential application as site directing carrier for ETO. The TGA data exhibited extent of grafting as 4% in case of MCM-41-A,20.19% in

PAA-MSNs and 23.75% in case of FA-MSNs respectively. The % loading and entrapment estimated by UV spectrophotometry is summarized in Table 6.4.

Sr No.	Sample	DRUG: MSN Ratio	Percentage Loading		Percentage Entrapment(%)
			By TGA	By UV	
1	ETO-MCM-41	1:1.5	38.93	39.22	98.18
2	ETO-MCM-41-A	1:1.5	36.20	37.19	91.29
3	ETO-PAA-MSN	1:1.5	31.05	32.08	80.30
4	ETO-FA-MSN	1:1.5	34.55	34.98	87.12

Table 6.4. Drug loading and % grafting of functional groups.

6.3.3 In vitro release study:

6.2.3.1 In vitro dissolution study

The dissolution profile of crystalline ETO, ETO-MCM-41, ETO-MCM-41-A and Marketed formulation (MF) in various media are presented in Fig 6.11 .

Appreciably, the rate of ETO release from MCM-41 was higher than that of plain crystalline ETO and MF. A remarkable dissolution enhancement of 5.1 times (from MCM-41) in comparison to plain ETO and 1.16 times in comparison to marketed formulation was obtained (at 45 min acetate media). Burst release was observed in case of unmodified MCM-41 with about 43 percent drug releasing in within the first 5 minutes, while when compared, a sustained release was obtained with MCM-41-A nanoparticles. This could be attributed to the fact that unmodified MCM-41 possess only silanol groups on the pore channel walls. These silanol groups form weak hydrogen bonds with ETO. To prevent this behaviour, the surface of MSNs was modified with amino groups on the pore channel walls. As evident, this provided a sustained release of ETO.

When compared the pore diameters of both nanoparticles, post surface modification, the pore diameter is decreased in case of MCM-41-A. This may be the explanation of difference in

release behaviour obtained in both the nanoparticles. Since, there is absence of any active carbonyl group on ETO, the probability of any chemical interaction on release behaviour can be ruled out. Thus, ultimately, decrease in pore diameter might be the probable reason for this. In all the media the observed dissolution rate of crystalline ETO was very low, reaching only 20 percent release on an average. In case of acetate not more than 16 percent ETO was accumulated. However, for all media tested, it could be concluded that overall for all the dissolution rate of ETO-MCM-41 was higher than plain ETO and MF. About complete drug release was obtained at 45 min in acetate media from MCM-41 NPs.

The remarkable improvement in dissolution could be credited to the mesopores of MSNs converting the crystalline state of ETO to a non-crystalline state, which is well known for improving the dissolution rate. The pores of MCM-41 are larger in comparison to MCM-41-A and ETO molecules adsorbed onto large mesopores have an added advantage and greater chance of escaping from these mesopore networks into the dissolution media. For MCM-41-A the diffusion of release medium into smaller pore mesopores, and counter diffusion of ETO from these mesopore channels are comparatively restricted resulting in the sustained slower release of ETO. Decrease in surface area is also observed post functionalization in case of MCM-41-A NPs. This could also be one of the reasons for aforementioned observations. Thus, amination led to prevention of the initial burst release of ETO. Ultimately, the ETO release rate decreases due to slow dissolution of ETO from pores of MCM-41-A. Hence, at about complete release from MCM-41, less than half amount of drug was released from MCM-41-A, into the release media. They can act as a promising oral sustained release system. The release of which can be modified just by simply controlling the grafting of amino groups. As, the difference in release is ultimately attributed to the functional groups on pore walls. As, there is an absence of weak hydrogen bond interactions, in MCM-41-A which were present in MCM-41. Moreover, stearic hindrance of alkyl chain would also be needed to be overcome.

Interestingly, the difference in release pattern was also depicted in dissolution kinetics. For ETO-MCM-41, Weibull model was found to be the best fit in all media (Table 6.5). This assessment was made based on three criteria, namely, Regression coefficient value, AIC and MSC values. As evident from the table 6.5 , AIC values were lowest for the best fit model i.e. Weibull in case of ETO-MCM-41. Also, this was supported by highest regression coefficient value and MSC values obtained for Weibull as compared to other models. However, as seen in Table 6.6. In case of MCM-41-A NPs Higuchi model was the appropriate one. Linear relationship between the fraction of release of ETO and square root of time, suggested a Higuchi diffusion process. This was again complementary to the AIC and MSC values obtained for Higuchi model.

The dissolution study carried out for studying the effect of food and enzymes on ETO release was successfully conducted (Fig 6.12). The dissolution data showed that there was almost a similar release in fed and fasted state gastric and intestinal dissolution media. This data complemented the conclusion that there was no effect of food (Fig 6.12). Interestingly, it was also confirmed that there was no interaction between amine functionalization and gelatin shell of the capsule in the presence of enzyme. As the release rates did not differ much in simulated gastric and intestinal media in both absence and presence of enzymes.

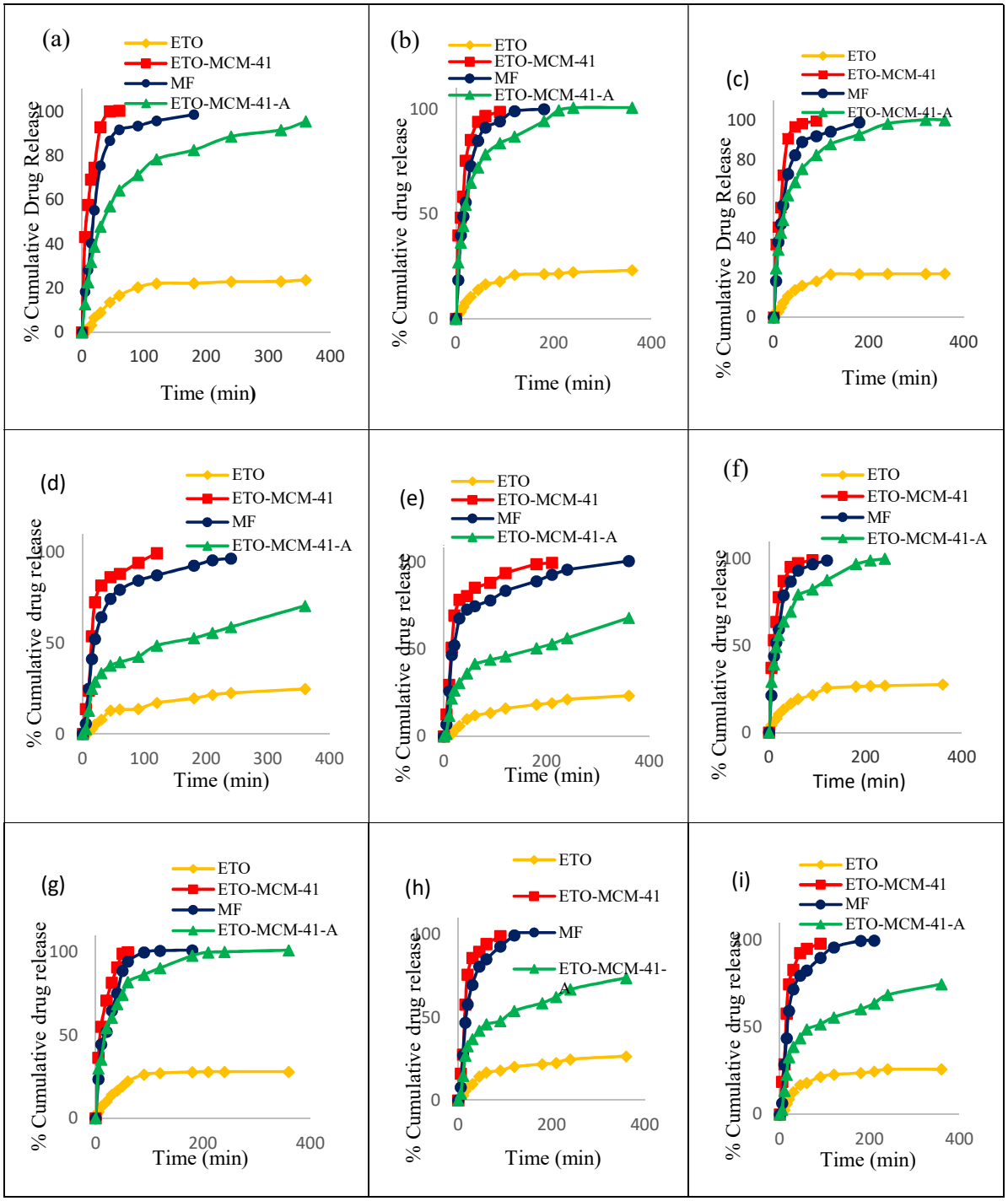

Figure 6.11. Dissolution profile or ETO, MF, ETO-MCM-41 and ETO-MCM-41-A in (a) Acetate; (b) SGF; (c) enzyme free SGF; (d) SIF; (e) enzyme free SIF; (f) FaSSGF; (g) FeSSGF; (h) FaSSIF; (i) FeSSIF

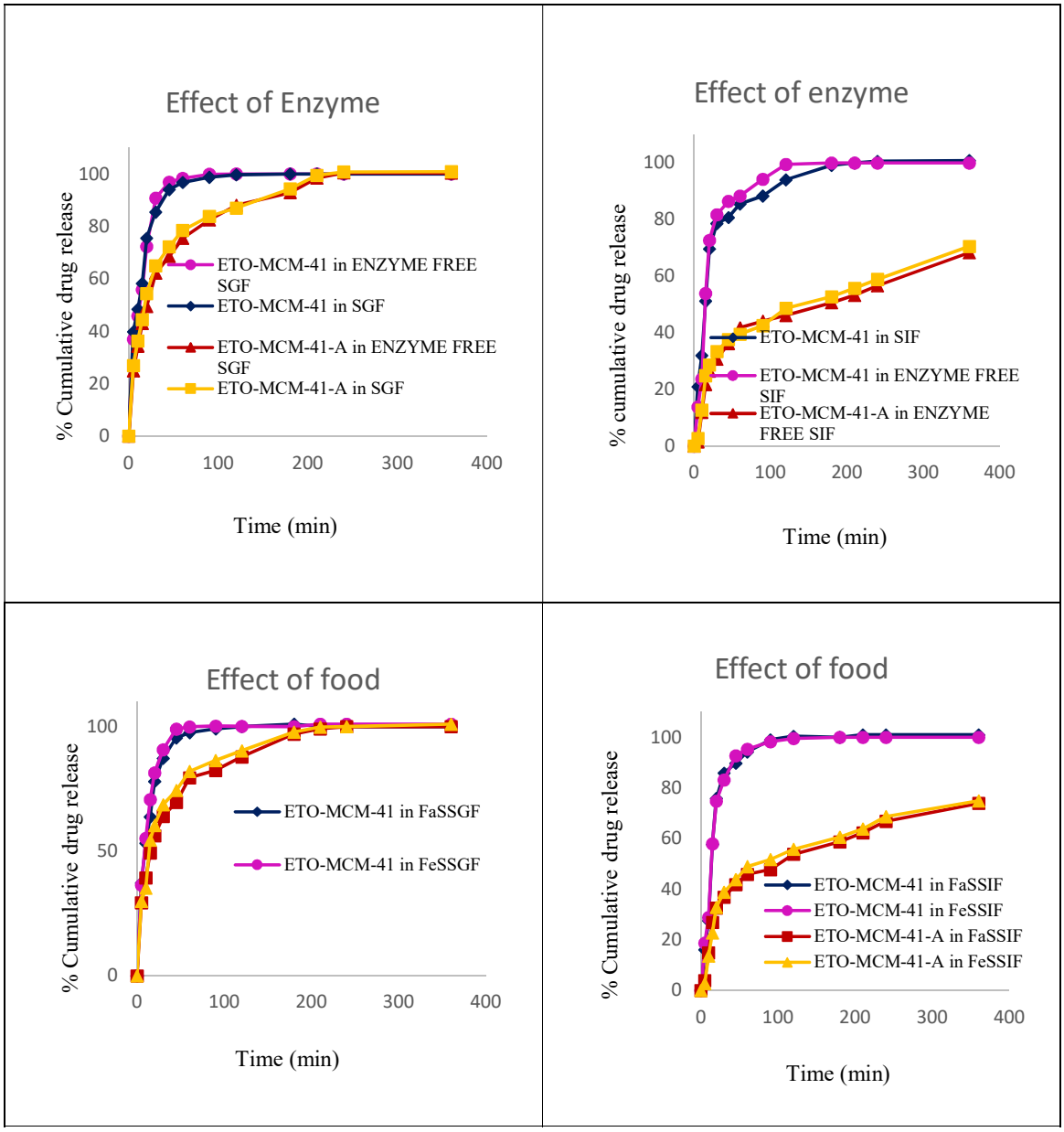

Figure 6.12. Graphs showing effect of food and enzyme on drug release from MCM-41 and MCM-41-A NPs.

Formulation	Statistical Parameters	Dissolution media	Dissolution model					
			Zero	First	Weibull	Higuchi	Hixon Crowell	Korsmeyer peppas
		A	0.3616	0.4948	0.8265	0.6034	0.4716	0.4605
		B	0.3165	0.7434	0.9431	0.5573	0.5756	0.4099
		C	0.3277	0.8326	0.9594	0.5690	0.6210	0.4222
		D	0.4843	0.8708	0.9560	0.7190	0.7807	0.5871
MCM-41	$.R^2$	E	0.5066	0.9009	0.9561	0.7419	0.8417	0.6093
		F	0.5302	0.8493	0.9225	0.7790	0.8636	0.6418
		G	0.3101	0.6156	0.8841	0.5503	0.4956	0.4031
		H	0.4318	0.7946	0.9505	0.6723	0.7036	0.5386
		I	0.4132	0.8714	0.9584	0.6534	0.7080	0.5149
		A	137.84	67.30	32.83	123.90	123.68	108.91
		B	110.54	41.98	39.67	95.03	91.87	81.72
		C	111.02	55.75	50.86	81.53	71.05	76.96
		D	107.61	70.62	59.32	91.76	86.23	87.06
MCM-41	AIC	E	118.60	75.45	72.004	101.84	96.88	92.83
		F	111.65	33.46	34.05	96.73	94.62	80.25
		G	82.49	44.06	42.30	65.05	56.48	56.37
		H	94.95	61.84	59.15	79.94	68.47	78.10
		I	109.43	64.12	62.12	94.01	87.27	88.92
		A	-1.55	3.87	5.43	-0.48	-0.46	0.66
		B	-1.27	4.16	5.49	0.13	0.41	1.34
		C	-1.11	3.33	3.82	0.75	1.80	1.21
		D	-0.68	2.67	2.89	0.75	1.25	1.18
MCM-41	MSC	E	-0.80	2.78	3.07	0.58	1.00	1.33
		F	-1.44	5.60	5.89	-0.14	0.04	1.35
		G	-0.68	3.58	3.87	1.25	2.20	2.21
		H	-0.47	2.84	3.10	1.03	2.17	1.21
		I	-0.89	3.22	3.40	0.50	0.97	1.12

A= Acetate media, B= SGF, C= SGF (Enzyme free), D= SIF, E= SIF (Enzyme free), F = Fast state simulated gastric fluid (FaSSGF), G= Fed state simulated gastric fluid (FeSSGF), H= Fast state simulated intestinal fluid (FaSSIF), I= Fed state simulated intestinal fluid (FeSSIF).

Table 6.5. Statistical analysis of release profile of ETO-MCM-41

Formulation	Statistical Parameters	Dissolution media	Dissolution model					
			Zero	First	Weibull	Higuchi	Hixon Crowell	Korsmeyer peppas
		A	0.7212	0.9011	0.9183	0.9359	0.9264	0.9159
		B	0.5778	0.9014	0.9244	0.9451	0.8394	0.7714
		C	0.6089	0.6089	0.9180	0.9359	0.8576	0.8377
		D	0.7991	0.8985	0.8556	0.9493	0.8698	0.9197
MCM-41-A	R^2	E	0.7442	0.8625	0.7626	0.9028	0.8272	0.8028
		F	0.5297	0.8989	0.9129	0.9374	0.8106	0.7714
		G	0.5314	0.9021	0.9066	0.9331	0.8108	0.7739
		H	0.7861	0.8931	0.8334	0.9323	0.8634	0.9273
		I	0.8240	0.9292	0.8763	0.9558	0.9027	0.9438
		A	121.28	85.35	97.51	55.47	95.43	100.34
		B	140.56	92.35	119.68	61.80	120.43	90.81
		C	111.02	91.68	107.36	45.91	106.46	82.04
		D	118.84	108.75	91.96	67.09	112.13	82.67
MCM-41-A	AIC	E	118.11	108.53	91.91	63.23	111.78	84.40
		F	126.82	89.48	96.01	56.83	104.69	73.48
		G	127.23	83.34	105.83	58.25	99.78	79.67
		H	122.88	110.42	96.97	64.10	114.52	85.29
		I	123.94	110.16	98.91	59.27	114.70	90.31
		A	-0.25	2.51	1.79	4.80	1.73	1.32
		B	-1.04	2.40	0.45	4.58	0.39	2.51
		C	-1.11	2.50	0.67	5.40	0.74	2.62
		D	-0.09	0.62	1.82	3.60	0.38	2.49
MCM-41-A	MSC	E	-0.06	0.61	1.80	3.85	0.36	2.34
		F	-0.95	1.91	1.04	4.42	0.74	3.14
		G	-0.96	2.41	0.68	4.24	1.15	2.69
		H	-0.23	0.65	1.61	3.96	0.36	2.45
		I	-0.18	0.79	1.60	4.43	0.47	2.21

A= Acetate media, B= SGF, C= SGF (Enzyme free), D= SIF, E= SIF (Enzyme free), F = Fast state simulated gastric fluid (FaSSGF), G= Fed state simulated gastric fluid (FeSSGF), H= Fast state simulated intestinal fluid (FaSSIF), I= Fed state simulated intestinal fluid (FeSSIF).

Table 6.6. Statistical analysis of release profile of ETO-MCM-41-A

5.2.3.1 In vitro diffusion study

The release behaviour of ETO-MCM-41 and ETO-PAA-MSN was investigated as a function of time at various pH 5.6, 6.8 and 7.4. ETO-PAA-MSN exhibited a pH dependent release behaviour and release was inversely proportional to pH. At lowest pH of 5.6, the drug release was faster and maximum. At pH 7.4 pK_a of ETO and PAA is 9.8 and 4.8 respectively (38). At this pH, positively charged ETO will bind with negatively charged PAA forming ETO-MCM-41-PAA complex via strong electrostatic interactions. This fact supports the percentage cumulative release obtained at pH 5.6 of 85 percent, and that at pH 6.8 and 7.4 of 70.72 and 36.21 percent respectively. At lower acidic pH (5.6 and 6.8) PAA is protonised ultimately leading to dissociation of strong electrostatic interactions existing between ETO and PAA. Thereby, leading to enhanced release of ETO incorporated into MCM-41-PAA. At pH 7.4 strong electrostatic interactions with PAA would be present. This strong forces might be playing a role in hindering the drug release at higher pH.

The best fit model was found to be korsmeyer-peppas and the diffusion exponential value (n) was used for determination of type of release mechanism playing role in diffusion of ETO from mesoporous matrix. For ETO-PAA-MSN n value was found to be 0.52. The n value between 0.43 and 0.85 signals a non-fickian anomalous diffusion mechanism present. The anomalous diffusion was observed which combines both fickian and non-fickian release mechanisms. Fickian diffusion might be there due to weak interaction between the drug and the non-functionalized silica surface. The diffusion and swelling rated both are commensurable. In Anomalous transport, the velocity of solvent diffusion and the polymeric relaxation possess similar magnitudes (39). In primary case of Fickian diffusion, n=0.5 the drug release is extensively governed by diffusion. The solvent transport rate or diffusion is way higher than the polymeric chain relaxation process. In any case n value > 0.85 stands for a swelling controlled diffusion process, attributed to the expansion of polymer used (40). For fickian

diffusion ETO released is governed by diffusion and solvent transport rate or diffusion is much greater than the process of polymeric chain relaxation. Moreover, if n value is greater than unity, it signifies Super case II model (39). Thus, it can be assumed that for PAA-MSN the anomalous mechanism based drug release is controlled both by diffusion and polymer swelling. Furthermore, in case of ETO-MCM-41, not much pronounced pH dependent release was observed and the mechanism of release was Fickian. Thus, it could be observed that a pH selective and effective sustained release was obtained in case of ETO-MCM-41-PAA for greater than 72 h. A complete summary of release mechanisms is given in table 6.7.

High pay loading of ETO was obtained for FA-MSNs. The *in vitro* release profile of drug in different pH conditions exhibited a different behavior (Fig 6.13). ETO-MCM-41-A and ETO-FA-MSNs showed a pH dependent release pattern in neutral and acidic PBS. A more prominent pH responsiveness was observed in case of FA-MSN. However, ETO-MCM-41 were devoid of any pH responsive behaviour and did not give a differential release pattern. The release of ETO was found to be inversely proportional to pH in case of FA-MSN. More of ETO was released in acidic media as compared to higher pH media. At about 72 h also the drug release at pH 5.6 from FA-MSN was about 82% whereas at 7.4 pH it was only about 56%. To determine the release mechanism the data were fitted to korsmeyer peppas model and determined based on n values or the release index. For MCM-41 matrix the release mechanism was found to be fickian with n values equal to 0.389 and 0.419 at pH 5.5 and 7.4 respectively, while for MCM-41-A it was found to be anomalous and FA-MSN release n value imparted a super case II transport mechanism (Table 6.7). Hence, FA-MSNs can be effectively used for targeting cancer cells which or intracellular components like lysosome and endosome possessing lower pH than the normal healthy tissue.

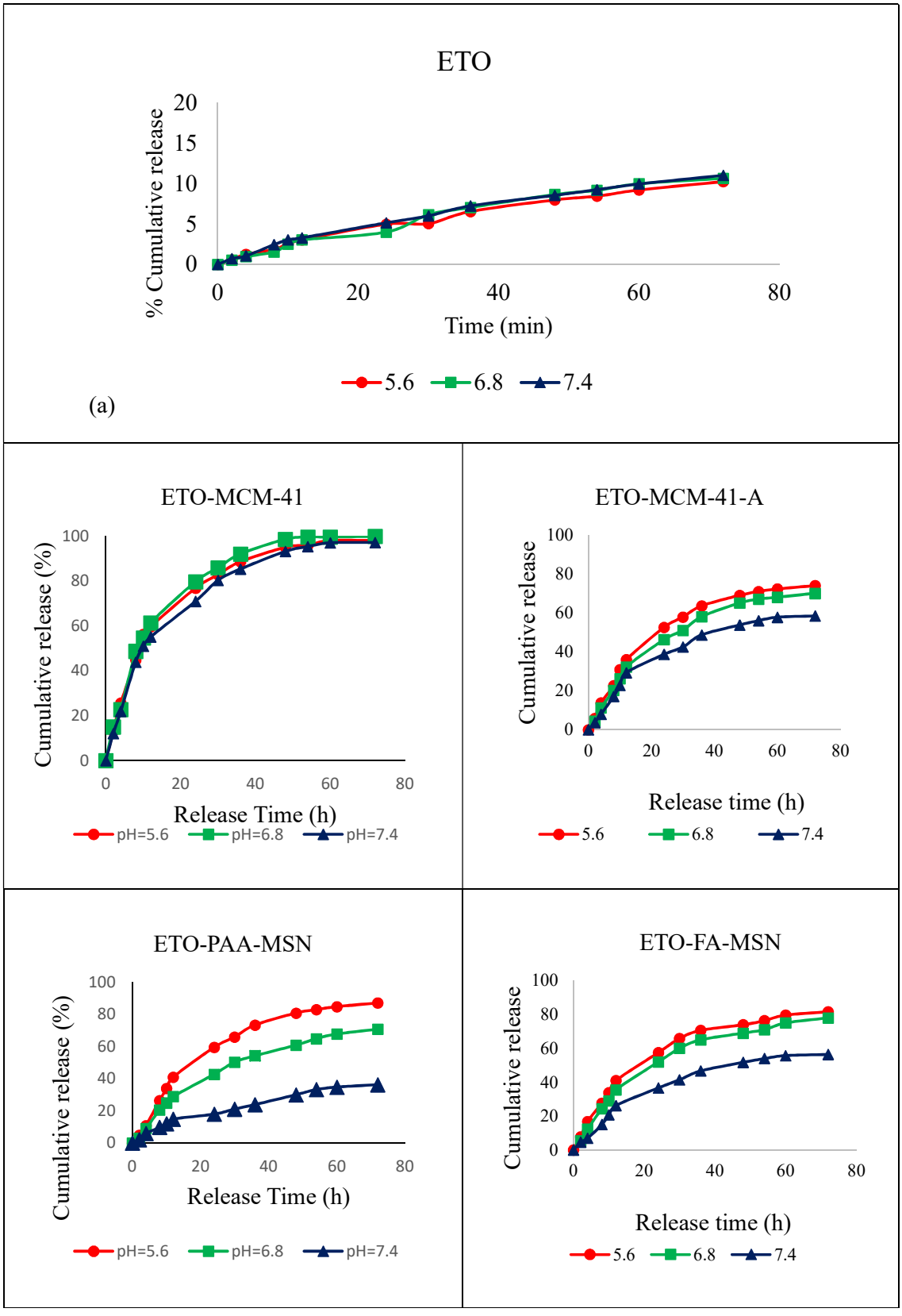

Figure 6.13. In vitro drug release from drug loaded bare and functionalized MSNs at different pH values.

Sr. No.	FORMULATION	pH	PARAMETERS	MODEL				
				Korsmeyer Peppas	transport mechanism	Zero order	First order	Higuchi
1.	ETO-MCM-41	5.6	R^2	0.9587		0.4381	0.9371	0.9282
			AIC	86.72		118.65	93.15	91.92
			MSC	2.53		0.0749	1.92	2.13
			n	0.389	Fickian			
2.	ETO-MCM-41	6.8	R^2	0.9540		0.4386	0.9357	0.9246
			AIC	89.00		119.51	98.15	93.41
			MSC	2.42		0.0808	1.95	2.088
			n	0.392	Fickian			
3.	ETO-MCM-41	7.4	R^2	0.9665		0.5383	0.9307	0.9518
			AIC	84.20		116.04	91.32	86.67
			MSC	2.76		0.300	1.80	2.558
			n	0.419	Fickian			
4.	ETO-PAA-MSN	5.6	R^2	0.9659		0.7645	0.9561	0.9642
			AIC	80.663		105.81	103.90	82.67
			MSC	2.8847		1.067	1.990	2.752
			n	0.532	anomalous			
5.	ETO-PAA-MSN	6.8	R^2	0.9816		0.8317	0.9724	0.9739
			AIC	68.4409		95.1815	71.68	70.94
			MSC	3.82		1.4177	3.224	3.281
			n	0.573	anomalous			
6.	ETO-PAA-MSN	7.4	R^2	0.9893		0.8880	0.9362	0.9720
			AIC	42.888		71.459	64.193	53.455
			MSC	4.029		1.8319	2.394	3.2168
			n	0.619	anomalous			
7.	ETO-MCM-41-A	5.6	R^2	0.9546		0.7145	0.9501	0.8851
			AIC	80.49		103.61	85.24	91.78
			MSC	2.53		0.8506	2.02	1.76
			n	0.485	anomalous	-	-	-
8.	ETO-MCM-41-A	6.8	R^2	0.9721		0.7806	0.9599	0.8590
			AIC	72.93		98.88	76.79	93.13
			MSC	3.13		1.13	2.83	1.577
			n	0.538	anomalous			
9.	ETO-MCM-41-A	7.4	R^2	0.9696		0.7692	0.9218	0.8614
			AIC	70.59		94.96	80.89	88.34

			MSC	2.95		1.084	2.16	1.59
			n	0.532	anomalous			
10.	ETO-FA-MSN	5.6	R^2	0.9632		0.6759	0.9539	0.9009
			AIC	81.06		107.19	88.65	91.78
			MSC	2.72		0.7049	2.42	1.89
			n	0.470	anomalous			
11.	ETO-FA-MSN	6.8	R^2	0.9609		0.6798	0.9586	0.8324
			AIC	70.51		94.89	72.95	87.12
			MSC	3.002		0.97	2.81	1.61
			n	0.520	anomalous			
12.	ETO-FA-MSN	7.4	R^2	0.9724		0.7952	0.9315	0.8477
			AIC	68.55		92.62	78.39	88.78
			MSC	3.06		1.212	2.307	1.508
			n	0.551	anomalous			

Table 6.7. Statistical analysis of diffusion release profile of ETO-MSNs

6.3.4 In vitro cytotoxicity study

In vitro cell cytotoxicity of ETO, ETO-MCM-41 and ETO-PAA-MSN was studied on prostate cancer cell lines androgen dependent LNCaP and androgen independent PC-3 at various concentration. PC-3 and LNCaP are the two most commonly used cell lines used in scientific studies for prostate cancer research. The cell cytotoxicity study was performed by MTT assay. Concentration dependent and time dependent study was conducted by MTT assay and percentage cell viability was determined. Different concentration of NPs and ETO were incubated for different time periods. Cytotoxicity of PAA-MSN carrier on both the cell lines was studied for concentration range of 0.1 to 100 µg/mL with incubation times of 24 and 72h respectively Fig 6.14 (a) (b). No significant cytotoxicity of carrier was observed with cell viability up to 91 % after 72h in 100 µg/mL observed (Fig 6.14 (a, b)). These results suggest good biocompatibility and suitability of PAA-MSN as a platform for delivery of anti-cancer drugs.

The concentration range selected for PC-3 cell lines was 0.1-20 µg/mL and 2 µg/mL to 60 µg/mL for LNCaP cells. The IC 50 values of free ETO on PC-3 and LNCaP were determined

as 23.85 µg/mL and 16.67 µg/mL for 24 h and 39.24 µg/mL and 22.03 µg/mL for 72h respectively. A remarkable reduction in IC_{50} values were observed for formulation (ETO-PAA-MSN). The IC_{50} values for ETO-PAA-MSN on PC-3 were 7.2 µg/mL and 3.56 µg/mL for 24h and 72h respectively and on LNCaP were 15.41 µg/mL and 4.28 µg/mL for 24h and 72h respectively. The cell viability was highly decreased in both the cell lines, exhibiting the effectiveness of developed MSNs in killing cancer cells. The percentage viability decreased with increase in concentration and time as displayed in Fig 6.14 (c) and (d).

In vitro cell cytotoxicity on both prostate cancer cell lines was evaluated by MTT assay. ETO loaded MSNs exhibited a dose dependent cytotoxicity after 24 and 72 h (Fig 6.15). Overall all the ETO loaded MSNs displayed more cytotoxicity than free ETO. Solubility limitations of ETO could be contributors towards its poor internalization into cells. But positive uptake of MSNs may solve this problem efficiently. Targeted ETO-FA-MSN showed a higher toxicity than their counterparts ETO-MCM-41 and ETO-MCM-41-A on both LNCaP and PC-3 cell lines. The success of ETO-FA-MSN was confirmed further by cellular uptake and apoptosis study. The cytotoxicity data for blank carriers MCM-41, MCM-41-A and FA-MSN revealed no toxicity on both the cell lines and it proved that all the MSNs were biocompatible and non-toxic to LNCaP and PC-3 cells. Comprehensively, results attest to the talent of ETO-FA-MSNs for ETO delivery by enhanced effectiveness of targeted delivery.

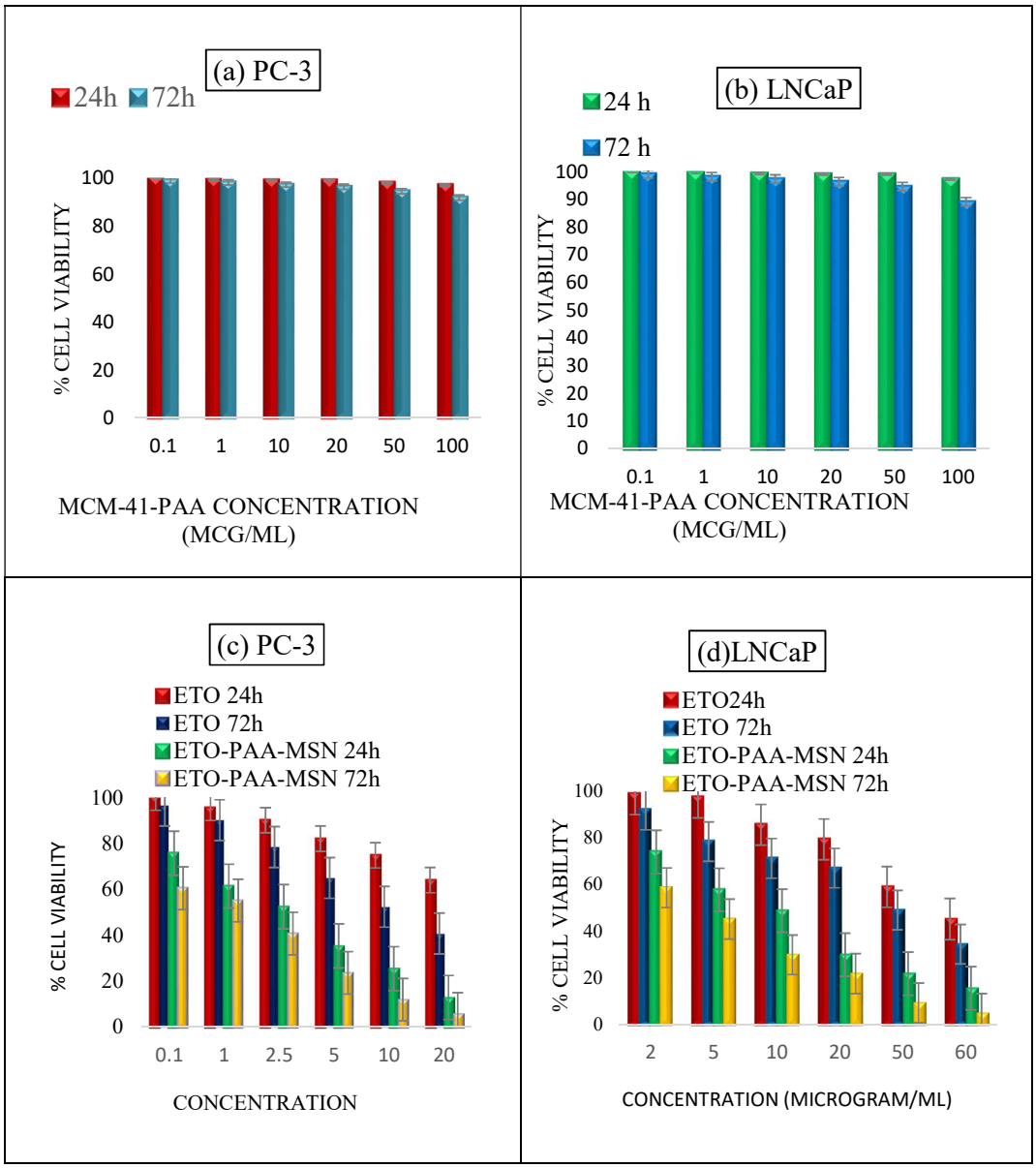

Figure 6.14. In vitro cell cytotoxicity assay (MTT assay) results showing effect of developed nanocarriers and formulation on Prostate cancer cell lines (PC-3 and LNCaP).

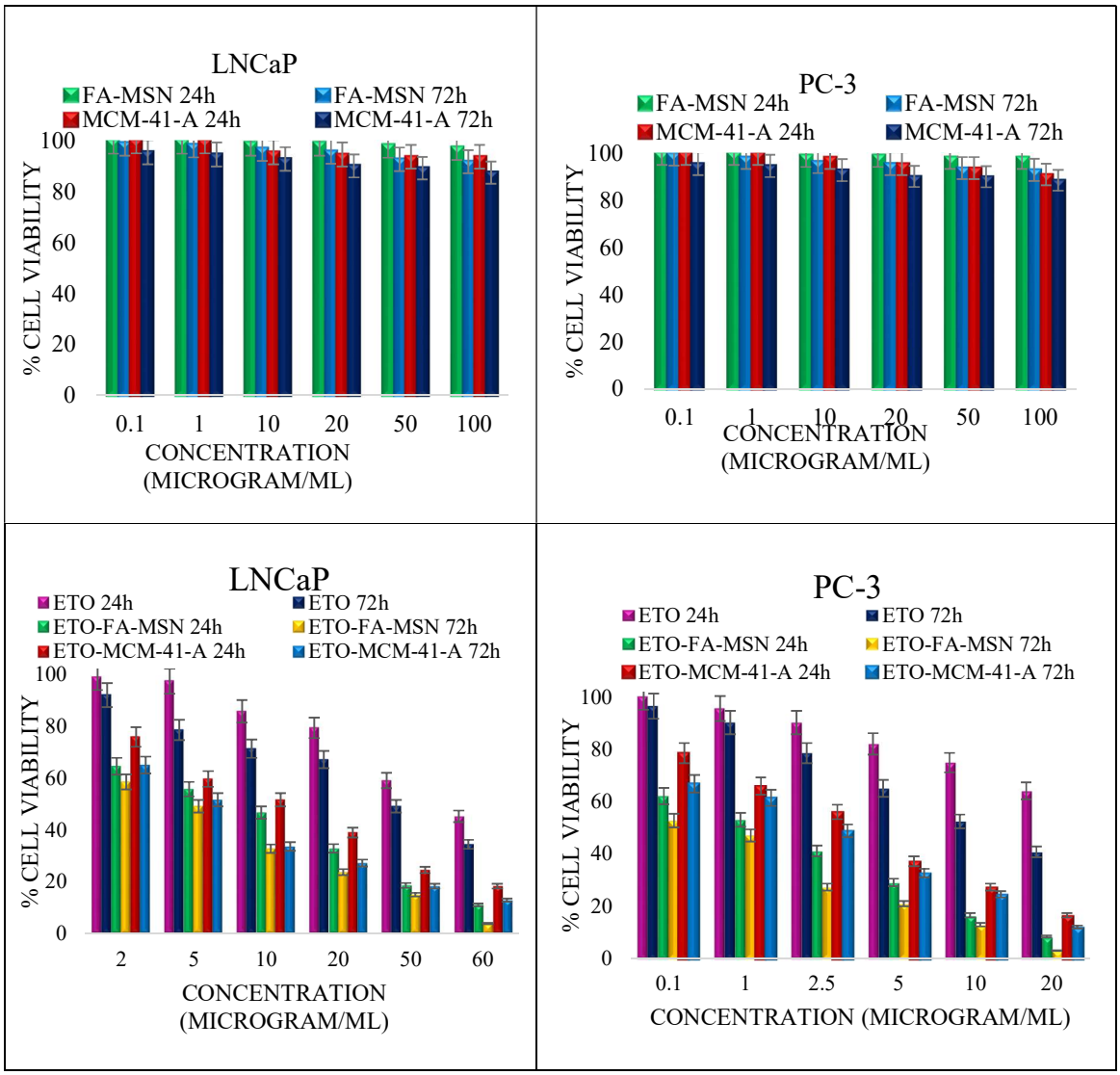

Figure 6.15. In vitro cell cytotoxicity assay (MTT assay) results showing effect of developed nanocarriers FA-MSNs and formulation on Prostate cancer cell lines (PC-3 and LNCaP).

6.3.5 Caco-2 monolayer cell line permeability study:

From the results obtained in cell cytotoxicity assay concentration of 100 µg/mL was selected to be safe for proceeding further with cell permeability study. Experiment was conducted for ETO, ETO loaded MCM-41 and ETO-MCM-41-A from apical to basal compartment. P_{app} value was estimated for various formulations (Table 6.8). There was an improvement of 4.66-fold in permeability of with respect to drug alone. Therefore, it could be concluded that ETO encapsulation into the mesoporous network proved to be beneficial in enhancing its

permeability as well (figure 6.16).

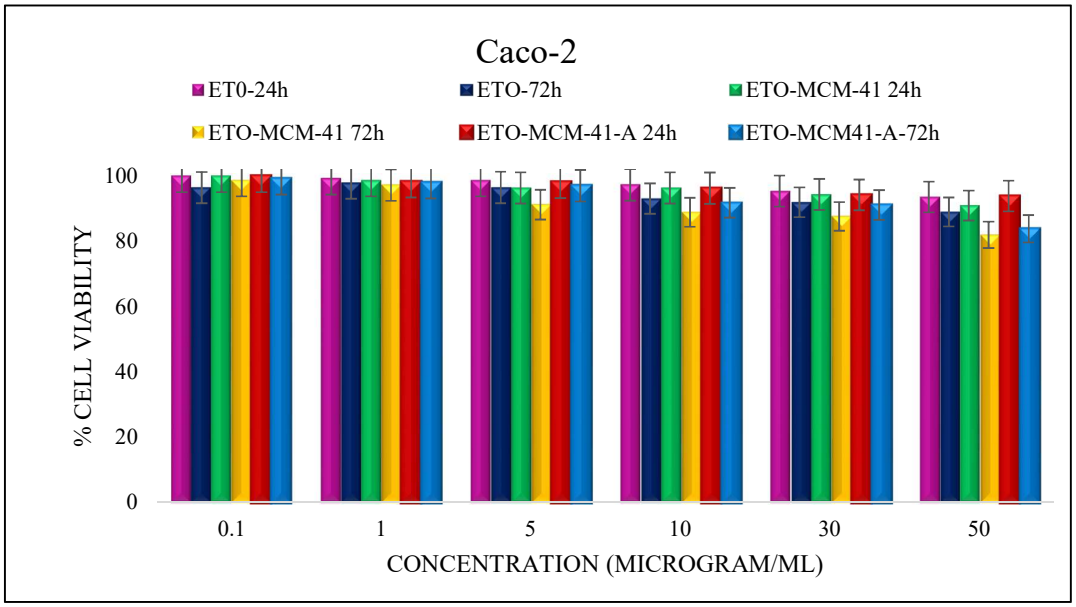

Figure 6.16. MTT assay on Caco-2 cells

Sr No	Time (min)	ETO	ETO-MCM-41	ETO-MCM-41-A
1	30	0.71	5.31	3.88
2	60	0.66	10.77	7.31
3	90	3.94	16.24	10.56
4	120	5.93	23.84	15.39
5	180	7.11	35.19	22.47
6	240	9.87	48.56	27.35
	dQ/dt	**0.0385**	**0.2049**	**0.1193**
	P_{app}	**2.046×10^{-2}**	**1.087×10^{-1}**	**6.33×10^{-2}**

Table 6.8 Permeability determination of developed formulations

6.3.6 In vitro cellular uptake study

6.3.6.2 Intracellular qualitative uptake study by confocal microscopy

Confocal microscopy images (Fig 6.17 and 6.18) showed successful increased time dependent uptake of FITC labelled PAA-MSNs and FA-MSNs as compared to MCM-41-A-MSNs in both LNCaP and PC-3 cells. A-MSNs showed a lower uptake with low visible green fluorescence. Enhanced fluorescence intensity was visible in the perinuclear region. A slightly higher uptake was visible in PC-3 cells than LNCaP. It is vital to deliver the cargo to the right destination and FCM analysis was useful in determining and quantifying the cellular uptake of MSNs in both prostate cancer cells. Here as well the empty nanovehicles were successful in uptake by LNCaP and PC-3 cells and localized effectively in the cytoplasm. Effective internalization and intracellular drug release were obtained by FA surface attachment and it acted as a suitable target specific ligand. This could lead to a slow and prolonged ETO accumulation into the cells. Figure 6.18 shows FITC#FA-MSNs having more rapport for both cells than FITC#A-MSNs.

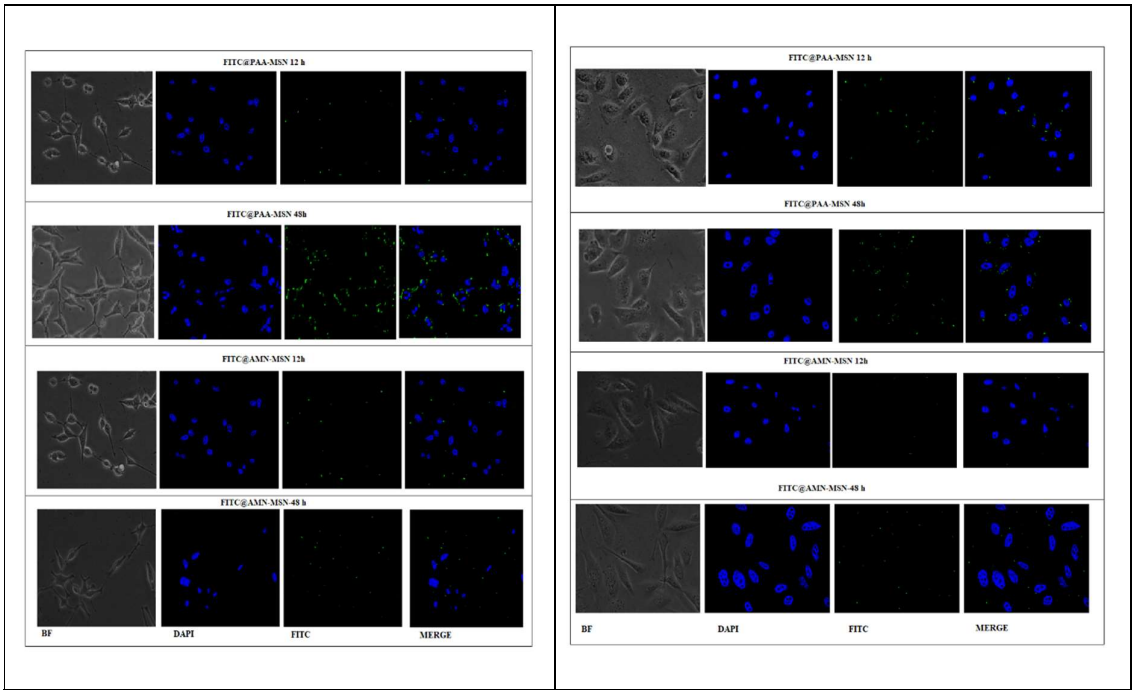

Figure 6.17. Confocal microscopic images of cellular uptake of FITC labelled PAA-MSNs (green) in LNCaP and PC-3 cell line with DAPI nuclear staining(blue)

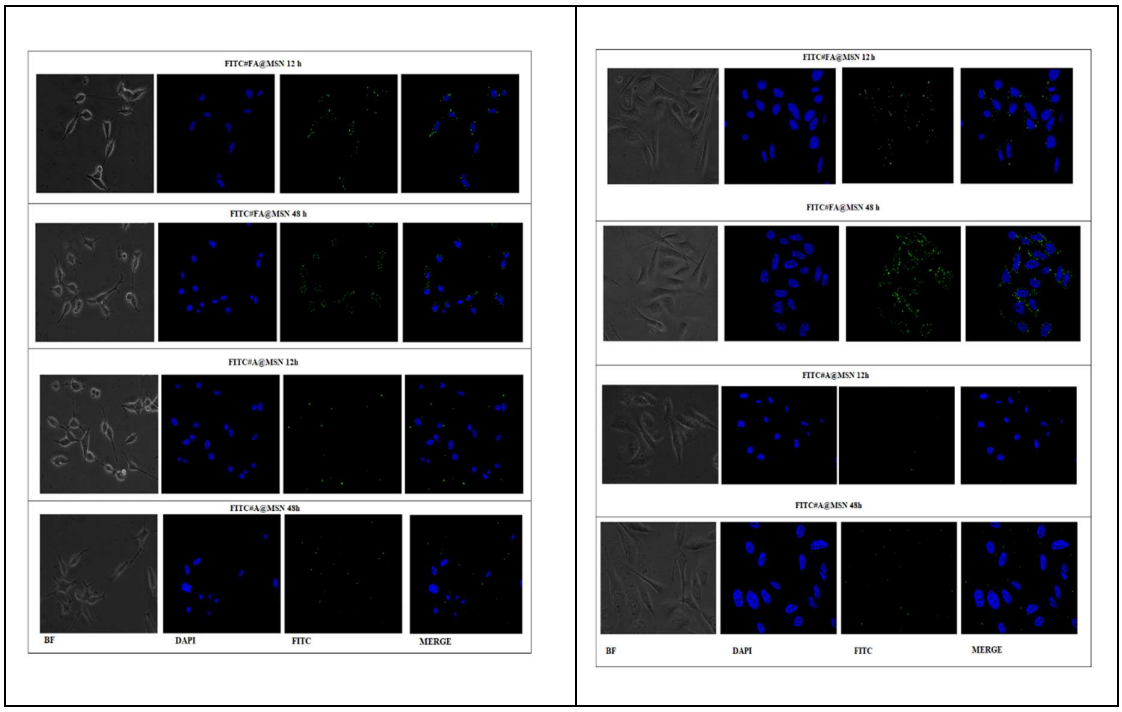

Figure 6.18. Confocal microscopic images of cellular uptake of FITC labelled FA-MSNs (green) in LNCaP and PC-3 cell line with DAPI nuclear staining(blue)

6.3.6.3 Intracellular quantitative uptake study by Flow cytometry

Confocal microscopy images showed an increase in the time dependent uptake of FITC labelled PAA-MSNs as compared to MCM-41-A MSNs in both LNCaP and PC-3 cells. MCM-41-A showed a lower visible green fluorescence indicating fewer uptake. Enhanced fluorescence intensity was visible in the perinuclear region. A slightly higher uptake was visible in LNCaP cells than PC-3. It is vital to deliver the cargo to the right destination and FCM analysis was useful in determining and quantifying the cellular uptake of MSNs in both prostate cancer cells. The empty nanovessels effectively localized in the cytoplasm. Effective internalization and intracellular drug release could be obtained by PAA surface enhancement. This could lead to a slow and prolonged ETO accumulation into the cells. Figure 6.19 shows FITC#PAA-MSNs exhibiting more uptake for both cells as compared to FITC#MCM-41-A. For LNCaP cells MCM-41-A MSNs showed 23.74% and FITC#PAA-MSNs showed a high cellular uptake of 84.22% respectively post 48 h. Similar trend was obtained for PC-3 cells with uptake of MCM-

41-A MSNs and PAA-MSNs at 24.83% and 80.86% respectively. For LNCaP cells A-MSNs showed 23.74% and FITC#FA-MSNs showed a high cellular uptake of 87.72% respectively post 48 h. Similar trend was obtained for PC-3 cells. Moreover, it was found that the uptake was less in both cell lines when treated with free FA+ FITC#FA-MSNs. This might be attributed to occupying of folate receptors by free FA before FA-MSNs, leaving lesser empty spaces for NPs.

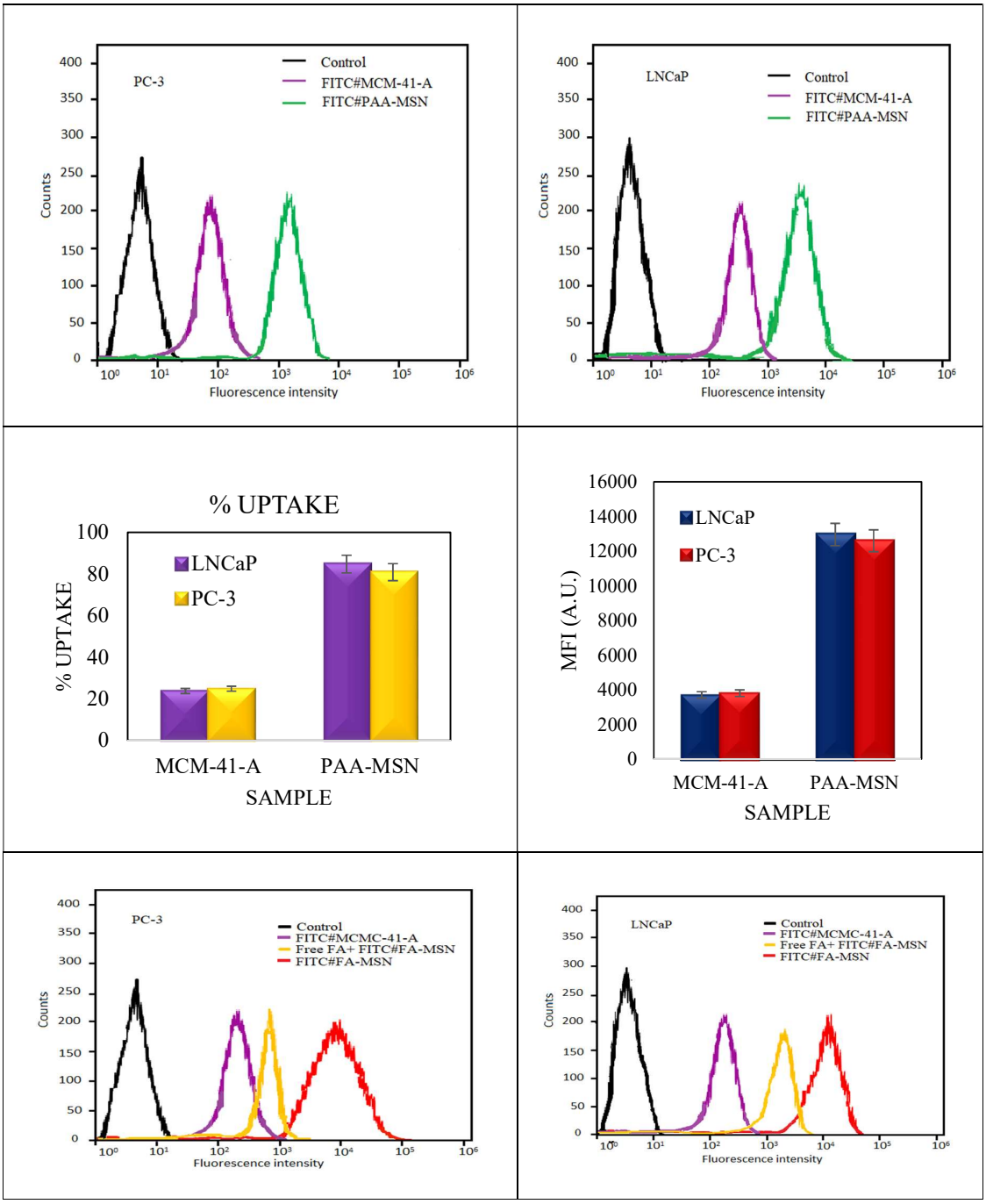
PC-3
Control
FITC#MCM-41-A
FITC#PAA-MSN
Counts
Fluorescence intensity
LNCaP
Control
FITC#MCM-41-A
FITC#PAA-MSN
Counts
Fluorescence intensity
% UPTAKE
% UPTAKE
LNCaP
PC-3
MCM-41-A
PAA-MSN
SAMPLE
MFI (A.U.)
LNCaP
PC-3
MCM-41-A
PAA-MSN
SAMPLE
PC-3
Control
FITC#MCMC-41-A
Free FA+ FITC#FA-MSN
FITC#FA-MSN
Counts
Fluorescence intensity
LNCaP
Control
FITC#MCMC-41-A
Free FA+ FITC#FA-MSN
FITC#FA-MSN
Counts
Fluorescence intensity

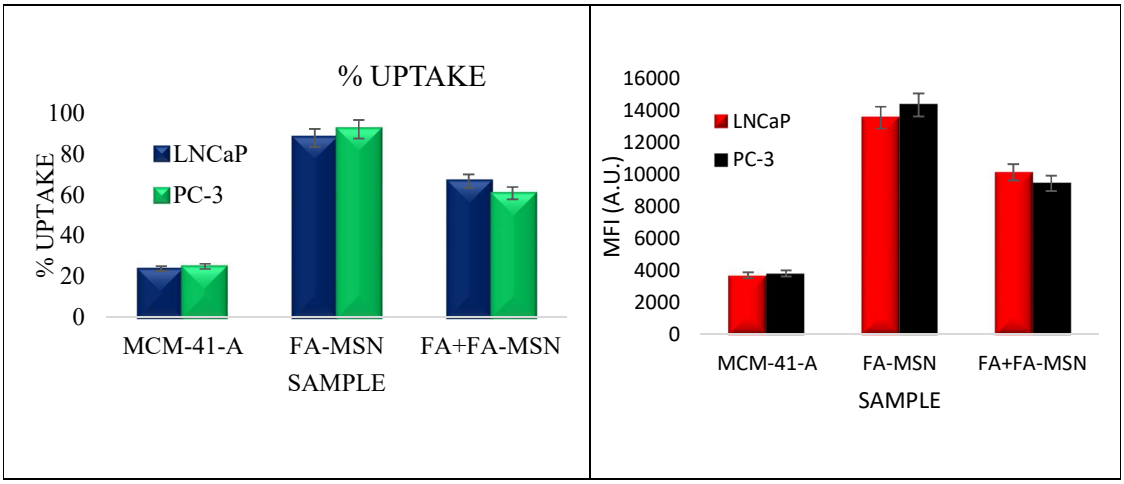

Figure 6.19. FACS study for synthesised MSNs

6.3.7 Evaluation of cell death mechanisms by apoptosis assay

The death mechanisms were adjudged by FACS protocol using Annexin V-FITC apoptosis detection kit. The cells were treated with ETO-MCM-41, ETO-MCM-41-A, ETO-PAA-MSN,ETO-FA-MSN NPs and free ETO for 24h. For LNCaP cells, total apoptosis was observed as 24.84%,55.62 %, 72.13% and 80.26% in cells treated with ETO-MCM-41, ETO-MCM-41-A, ETO-PAA-MSN and ETO-FA-MSN respectively. For PC-3 cells total apoptosis including early and late was 16.78%, 55.88%, 77.05% and 73.94% respectively for ETO-MCM-41, ETO-MCM-41-A, ETO-PAA-MSN and ETO-FA-MSNs. ETO could induce very less early apoptosis in the cells due to poor internalization into cells. Notably, drug loaded NPs led to early and late apoptosis induction in within 24 h in LNCaP cells. Remarkably FA-MSNs were capable of inducing both early and more late apoptosis at the same concentration (Figure 6.20). Also, they exhibited higher early and late apoptotic cells percentage than MCM-41-A NPs. It can be concluded that target group played a major role in giving this outcome. Almost similar results were obtained for PC-3 cells with more population found in late apoptotic stage than other MSNs or drug itself.

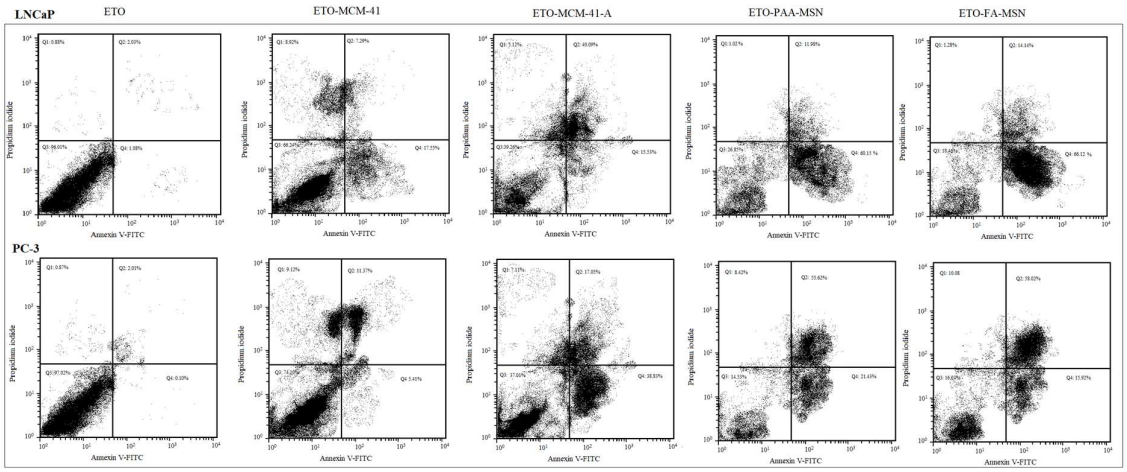

Figure 6.20. Apoptosis study of MSNs.

6.3.8 Haemolysis study

Hem compatibility is important and foremost requirement for systemic administration of NPs. Therefore, a hemolysis assay was performed to evaluate hem compatibility of MSNs. Biosafety of MSNs on RBCs was assessed by hemolysis assay (41, 42). All the synthesized MSNs were found to be highly hem compatible and exhibited very less haemolysis than free ETO and bare MSNs. Complete lysis was observed in Triton X-100 treated RBCs taken as positive control. ,ETO, ETO-MCM-41, ETO-MCM-41-A, ETO-PAA-MSN and ETO-FA-MSN exhibited 1.18, 2.62 0.98 and 1.09% haemolysis respectively. Further, FA-MSNs exposed RBCs maintained their biconcave disc shape. Surface coated MSNs were successful in maintaining the integrity of RBC membrane. Figure 6.21 shows in detail the microscopic and visual images of haemolysis study along with the UV-Vis spectra. The concentration range studied included 1-100 µg/mL. Predictably, Positive control (Triton X100 treated RBCs) displayed significant haemolysis. The ETO-MCM-41 and ETO-PAA-MSN NPs demonstrated exceptional hem compatibility similar to negative control (PBS 7.4). Overall the percentages obtained were well within the criteria of < 5 %.

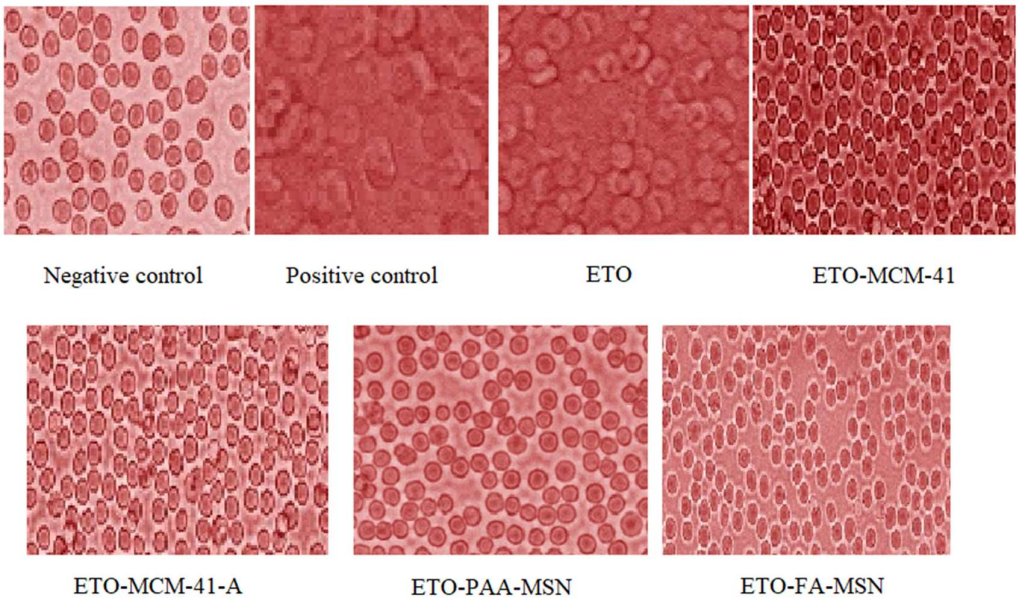

Figure 6.21. Microscopic images of Haemolysis study of MSNs

6.3.9 In vivo pharmacokinetic study

6.3.9.1 Pharmacokinetic study for oral formulation

The pharmacokinetic parameters of all the 3 different samples administered were quite different from each other(figure 6.22). Free ETO exhibited a more rapid clearance from blood with $t_{1/2}$ 6.88 min and AUC 12.44 µg/mL h. ETO loaded MCM-41 NPs also exhibited AUC 52.78 µg/mL h and a half-life of 12.12h (4.35 times) as compared to free ETO (table 6.9). Whereas, ETO-MCM-41-A exhibited a slow and steady clearance with longer $t_{1/2}$ 13.01h and AUC 30.05µg/mL h (2.47 times) as compared to free ETO and comparable to MF. ETO loaded nanocarriers had a slower plasma elimination rate and longer circulation time than ETO alone.

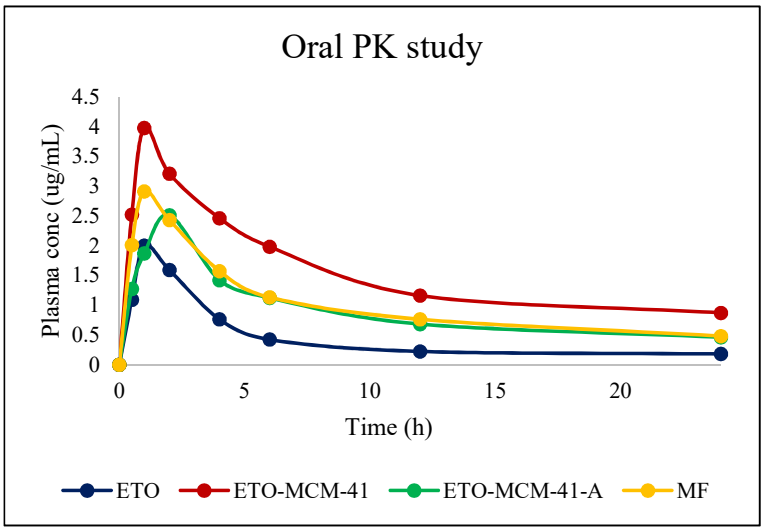

Figure 6.22. Oral pharmacokinetic data for ETO and ETO loaded MSNs

Parameters	$T_{1/2}$	T_{max}	C_{max}	AUC	MRT
ETOPOSIDE	6.88	1	2.06	12.44	10.61
ETO-MCM-41	12.12	1	3.98	52.78	18.23
ETO-MCM-41-A	13.01	2	2.51	30.05	17.97
M.F.	14.98	1	2.91	34.59	19.49

Table 6.9. Oral pharmacokinetic study of MSNs

6.3.9.2 Pharmacokinetic study for parenteral formulation

Statistically significant differences were found in the major pharmacokinetic parameters between ETO and formulations (Fig 6.23). Free ETO exhibited a more rapid clearance from blood with 2.85±1.6 $t_{1/2}$ and 59.37±1.2 AUC µg/mL h. ETO loaded PAA-MSNs exhibited the longest circulation time with plasma half-life of 14.59±0.5h. Whereas, ETO-FA-MSN exhibited a slow and steady clearance with longer $t_{1/2}$ and higher AUC (3.9 and 4.19 times) as compared to free ETO. Higher $t_{1/2}$ indicates the ability of nanocarriers to accumulate at tumor site and give enhanced therapeutic effect (Table 6.10). ETO loaded nanocarriers had a slower plasma elimination rate and longer circulation time than ETO alone.

The concentration of ETO in major organs was determined at 24 h (Fig 6.24). From results it could be inferred that concentration of PAA-MSNs and ETO-FA-MSNs in all major organs was remarkably decreased as compared to ETO alone. Thus, ETO NPs showed lower accumulation in all major organs than free ETO at all time points. This might be due to prolonged blood circulation of MSNs in bloodstream thus reducing major side effects associated with ETO.

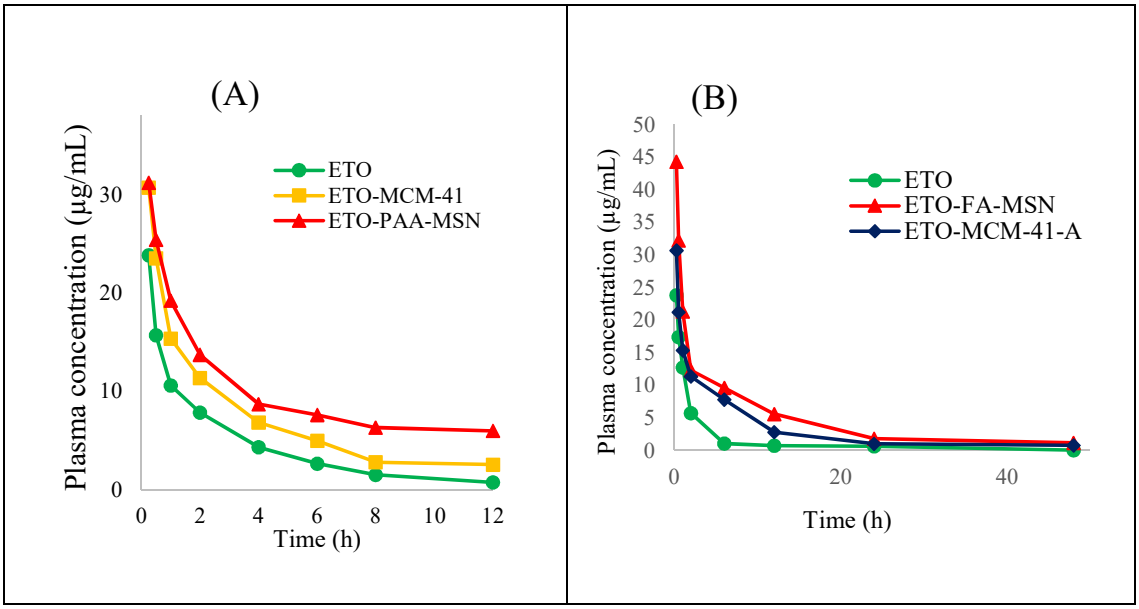

Figure 6.23. Intravenous Pharmacokinetic data for (A) ETO loaded MCM-41 PAA NPs and (B) ETO loaded MCM-41-FA NPs

Group	$t_{1/2}$ (h)	AUC $_{0-t}$ (µg/ml*h)	Cl (mg)/(µg/ml)/h	V_{ss} (mg)/(µg/ml)	MRT (h)	C_{max} (µg/ml)
ETO	2.85±1.6	59.37±1.2	0.1684±0.9	0.5897±0.6	3.50±0.9	23.86±0.6
ETO-MCM-41	6.93±0.9	135.77±1.4	0.0736±0.2	0.6344±1.3	8.61±0.7	28.34±0.2
ETO-PAA-MSN	14.59±0.5	246.70±1.2	0.0405±0.7	0.7692±1.1	18.97±1.4	31.22±0.5
ETO-FA-MSN	11.14±0.4	249.07±0.9	0.0401±0.1	0.5145±1.5	12.81±1.1	45.32±0.1

Table 6.10. Pharmacokinetic data of *i.v.* administered MSNs.

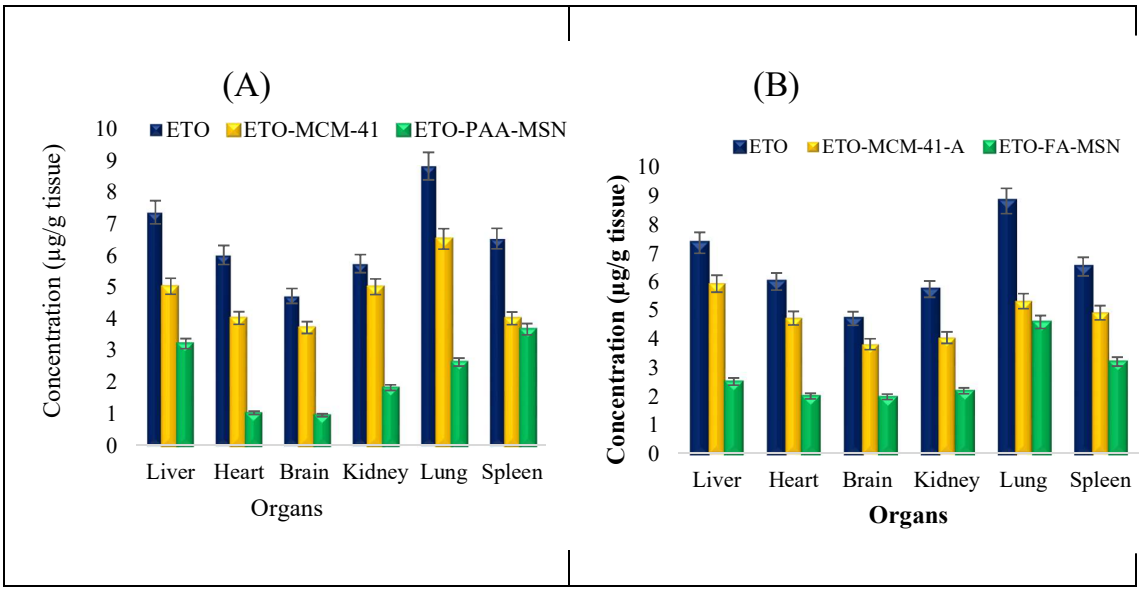

Figure 6.24. Biodistribution study results of the synthesized MSNs i.e. (A) ETO loaded MCM-41 PAA NPs and (B) ETO loaded MCM-41-FA NPs

The histological examination of various major organs post-formulation administration revealed no major toxicity (Fig 6.25). H&E sections of various organs of healthy swiss albino mice 24 h after intravenous administration are shown. Compared with the control group there were no major differences or inflammation observed in case of mice treated with ETO-PAA-MSNs and ETO-FA-MSNs even after 24h. A slight inflammation was observed in Liver tissue post 24 h free ETO administration indicating toxicity caused by drug.

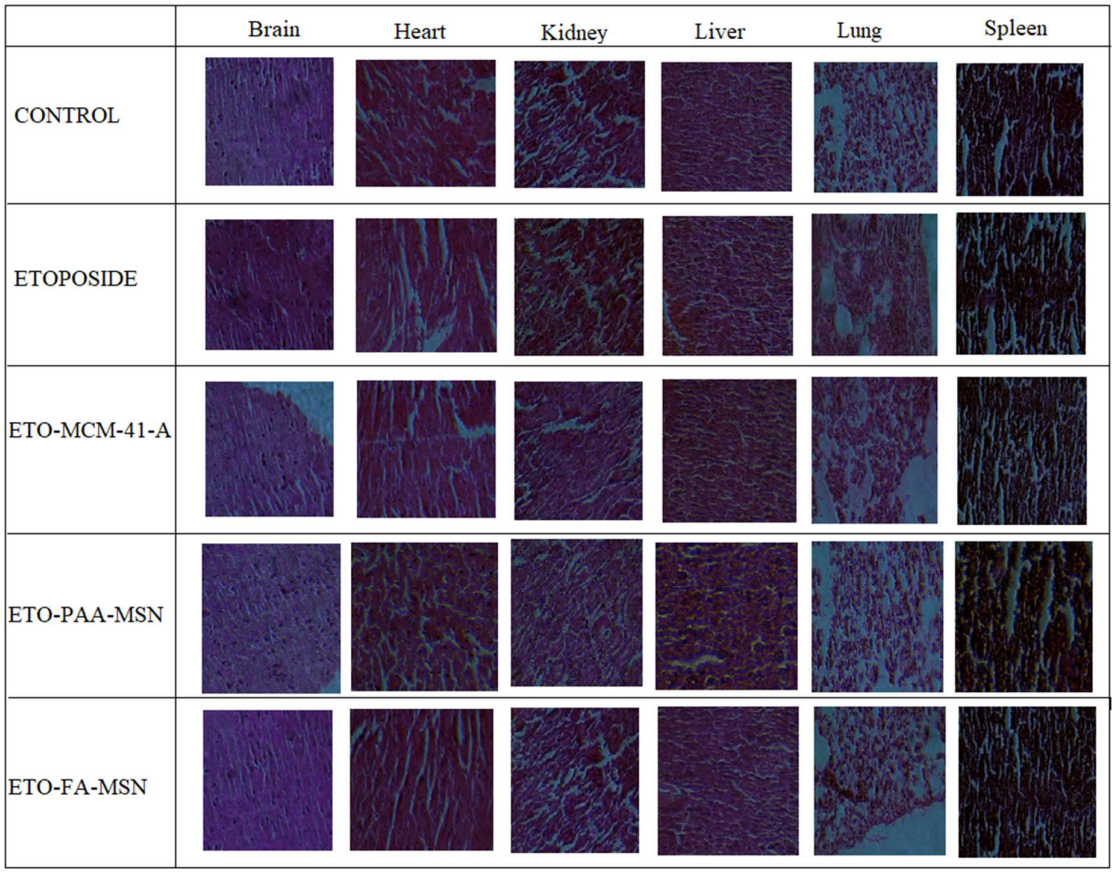

Figure 6.25. Histological examination of major tissue post administration of ETO and ETO loaded MSNs.

6.3.10 Stability study of mesoporous silica nanoparticles

The DSC (Figure 6.26) and SXRD data revealed that the synthesized MSNs were stable at 40±2 ºC and 75±5 %RH for the tested duration. The figure reveals no degradation or emergence of sharp peak in the drug loaded MSNs spectra suggesting absence of any drug leakage. Further, identical LXRD pattern at 0^{th} month and after 6^{th} month (Figure 6.27) revealed that the mesoporous skeleton was well intact.

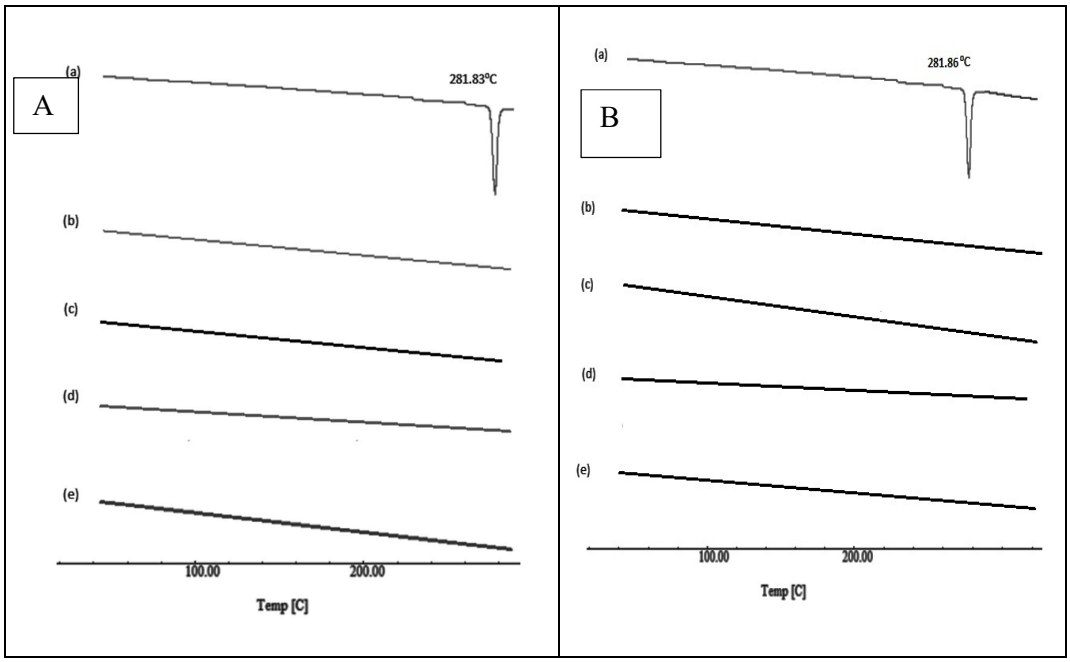

Figure 6.26. DSC thermogram of (a) ETO (b)ETO-MCM-41 (c) ETO-MCM-41-A (d) ETO-PAA-MSN (e) ETO-FA-MSN at 0^{th} and 6^{th} month

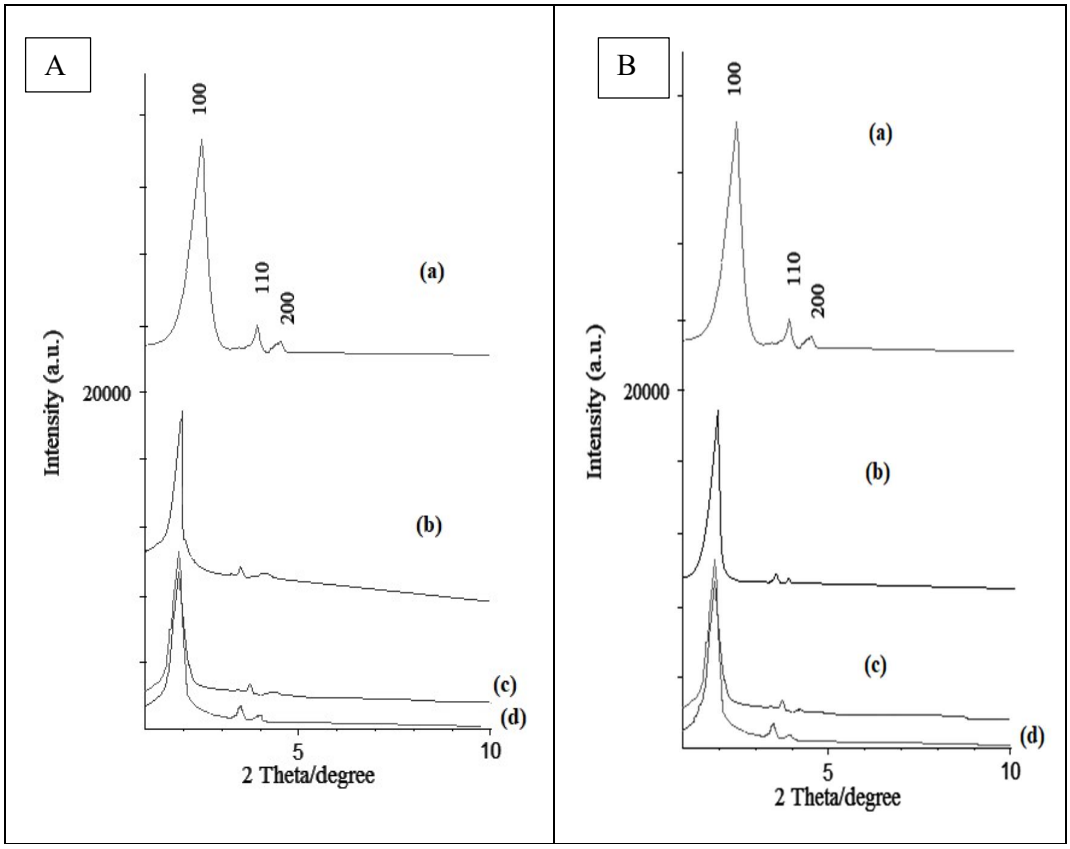

Figure 6.27. LXRD data for (a) ETO-MCM-41, (b) ETO-MCM-41-A (c) ETO-PAA-MSN and (d) ETO-FA-MSN at (A) 0^{th} and (B) 6^{th} month.

6.4 Conclusion

The results obtained from the entire study suggested that the ETO encapsulation into the MSN framework was successful and resulted in a marvellous enhancement in its dissolution rate (5.1 times) and bioavailability (4.35 times) in case of ETO-MCM-41. This in turn could lead to a significant dose reduction and it may be possible to achieve a greater efficacy with the lowest dose of drugs which suffer from solubility and permeability limitations. The targeting efficiency of MSNs also proved to be high as concluded from the enhanced cellular uptake of functionalized MSNs by both LNCaP and PC-3 prostate cancer cells as compared to bare MSNs. PAA-MSNs and FA-MSNs exhibited a significantly higher cellular uptake than MCM-41-A MSNs. Cellular uptake by LNCaP cells was 23.74 %, 84.22% and 87.72% for FITC#MCM-41-A, FITC#PAA-MSN and FITC#FA-MSN respectively. Cellular uptake by PC-3 cells was 24.83%, 80.86% and 91.87% for FITC#MCM-41-A, FITC#PAA-MSN and FITC#FA-MSN respectively. The most important aspect of a delivery system, the biosafety of MSNs was also established by haemolysis and histological examination. All the MSN formulations proved to be hem compatible and safe. This property of MSNs can prove to be a benchmark in cancer treatment as it will prove to be less toxic on healthy human organs at the same time efficient in accumulating the dose in the tumour cells. This will lead to diminished toxicities and overcome the drawbacks associated with chemotherapy at a greater extent.

6.5 References:

1. Hande K. Etoposide: four decades of development of a topoisomerase II inhibitor. European journal of cancer. 1998;34(10):1514-21.

2. KING MLS, SULLIVAN MM. The similarity of the effect of podophyllin and colchicine and their use in the treatment of condylomata acuminata. Science. 1946;104(2698):244-5.

3. Loike JD, Horwitz SB. Effects of podophyllotoxin and VP-16-213 on microtubule assembly in vitro and nucleoside transport in HeLa cells. Biochemistry. 1976;15(25):5435-43.

4. Chen AY, Liu LF. DNA topoisomerases: essential enzymes and lethal targets. Annual review of pharmacology and toxicology. 1994;34(1):191-218.

5. Froelich-Ammon SJ, Osheroff N. Topoisomerase poisons: harnessing the dark side of enzyme mechanism. Journal of Biological Chemistry. 1995;270(37):21429-32.

6. Slowing II, Vivero-Escoto JL, Wu C-W, Lin VS-Y. Mesoporous silica nanoparticles as controlled release drug delivery and gene transfection carriers. Advanced drug delivery reviews. 2008;60(11):1278-88.

7. Joo SH, Park JY, Tsung C-K, Yamada Y, Yang P, Somorjai GA. Thermally stable Pt/mesoporous silica core–shell nanocatalysts for high-temperature reactions. Nature materials. 2009;8(2):126.

8. Wu L, Jiao Z, Wu M, Song T, Zhang H. Formation of mesoporous silica nanoparticles with tunable pore structure as promising nanoreactor and drug delivery vehicle. RSC Advances. 2016;6(16):13303-11.

9. Lu J, Liong M, Li Z, Zink JI, Tamanoi F. Biocompatibility, biodistribution, and drug-delivery efficiency of mesoporous silica nanoparticles for cancer therapy in animals. Small. 2010;6(16):1794-805.

10. Engin K, Leeper D, Cater J, Thistlethwaite A, Tupchong L, McFarlane J. Extracellular pH distribution in human tumours. International Journal of Hyperthermia. 1995;11(2):211-6.

11. Lee ES, Oh KT, Kim D, Youn YS, Bae YH. Tumor pH-responsive flower-like micelles of poly (L-lactic acid)-b-poly (ethylene glycol)-b-poly (L-histidine). Journal of Controlled Release. 2007;123(1):19-26.

12. Yang JM, Huang MJ, Yeh TS. Preparation of poly (acrylic acid) modified polyurethane membrane for biomaterial by UV radiation without degassing. Journal of Biomedical Materials Research: An Official Journal of The Society for Biomaterials, The Japanese Society for Biomaterials, and The Australian Society for Biomaterials. 1999;45(2):133-9.

13. Tripathi SK, Ahmadi Z, Gupta KC, Kumar P. Polyethylenimine-polyacrylic acid nanocomposites: type of bonding does influence the gene transfer efficacy and cytotoxicity. Colloids and Surfaces B: Biointerfaces. 2016;140:117-20.

14. Yuan L, Tang Q, Yang D, Zhang JZ, Zhang F, Hu J. Preparation of pH-responsive mesoporous silica nanoparticles and their application in controlled drug delivery. The Journal of Physical Chemistry C. 2011;115(20):9926-32.

15. Xiao X, Liu Y, Guo M, Fei W, Zheng H, Zhang R, et al. pH-triggered sustained release of arsenic trioxide by polyacrylic acid capped mesoporous silica nanoparticles for solid tumor treatment in vitro and in vivo. Journal of biomaterials applications. 2016;31(1):23-35.

16. Li H, Yu H, Zhu C, Hu J, Du M, Zhang F, et al. Cisplatin and doxorubicin dual-loaded mesoporous silica nanoparticles for controlled drug delivery. RSC Advances. 2016;6(96):94160-9.

17. Hattori Y, Maitani Y. Folate-linked nanoparticle-mediated suicide gene therapy in human prostate cancer and nasopharyngeal cancer with herpes simplex virus thymidine kinase. Cancer gene therapy. 2005;12(10):796.

18. Martínez-Carmona M, Lozano D, Colilla M, Vallet-Regí M. Selective topotecan delivery to cancer cells by targeted pH-sensitive mesoporous silica nanoparticles. Rsc Advances. 2016;6(56):50923-32.

19. Singh R, Singh S, Sharma PK, Lillard Jr JW. T regulatory and prostate cancer cell-specific drug targeting using novel XPclad© nanoparticles (42.7). Am Assoc Immnol; 2009.

20. López V, Villegas MR, Rodriguez V, Villaverde G, Lozano D, Baeza A, et al. Janus mesoporous silica nanoparticles for dual targeting of tumor cells and mitochondria. ACS applied materials & interfaces. 2017;9(32):26697-706.

21. de Oliveira LFa, Bouchmella K, Gonçalves KdA, Bettini J, Kobarg Jr, Cardoso MB. Functionalized silica nanoparticles as an alternative platform for targeted drug-delivery of water insoluble drugs. Langmuir. 2016;32(13):3217-25.

22. Summerlin N, Qu Z, Pujara N, Sheng Y, Jambhrunkar S, McGuckin M, et al. Colloidal mesoporous silica nanoparticles enhance the biological activity of resveratrol. Colloids and Surfaces B: Biointerfaces. 2016;144:1-7.

23. Marques M. Dissolution media simulating fasted and fed states. Dissolution Technologies. 2004;11(2):16-9.

24. Vertzoni M, Dressman J, Butler J, Hempenstall J, Reppas C. Simulation of fasting gastric conditions and its importance for the in vivo dissolution of lipophilic compounds. European Journal of Pharmaceutics and Biopharmaceutics. 2005;60(3):413-7.

25. Shah PV, Rajput SJ. A comparative in vitro release study of raloxifene encapsulated ordered MCM-41 and MCM-48 nanoparticles: A dissolution kinetics study in simulated and biorelevant media. Journal of Drug Delivery Science and Technology. 2017;41:31-44.

26. Costa P, Lobo JMS. Modeling and comparison of dissolution profiles. European journal of pharmaceutical sciences. 2001;13(2):123-33.

27. Gayam SR, Wu S-P. Redox responsive Pd (II) templated rotaxane nanovalve capped mesoporous silica nanoparticles: a folic acid mediated biocompatible cancer-targeted drug delivery system. Journal of Materials Chemistry B. 2014;2(40):7009-16.

28. Kim TH, Kim M, Park HS, Shin US, Gong MS, Kim HW. Size-dependent cellular toxicity of silver nanoparticles. Journal of biomedical materials research Part A. 2012;100(4):1033-43.

29. Zhang Y, Zhi Z, Jiang T, Zhang J, Wang Z, Wang S. Spherical mesoporous silica nanoparticles for loading and release of the poorly water-soluble drug telmisartan. Journal of Controlled Release. 2010;145(3):257-63.

30. Heikkilä T, Salonen J, Tuura J, Hamdy M, Mul G, Kumar N, et al. Mesoporous silica material TUD-1 as a drug delivery system. International journal of pharmaceutics. 2007;331(1):133-8.

31. Kim JM, Chang SM, Kong SM, Kim K-S, Kim J, Kim W-S. Control of hydroxyl group content in silica particle synthesized by the sol-precipitation process. Ceramics International. 2009;35(3):1015-9.

32. Jaroniec C, Gilpin R, Jaroniec M. Adsorption and thermogravimetric studies of silica-based amide bonded phases. The Journal of Physical Chemistry B. 1997;101(35):6861-6.

33. Rashidi L, Vasheghani-Farahani E, Soleimani M, Atashi A, Rostami K, Gangi F, et al. A cellular uptake and cytotoxicity properties study of gallic acid-loaded mesoporous silica nanoparticles on Caco-2 cells. Journal of nanoparticle research. 2014;16(3):2285.

34. de Oliveira Freitas LB, Bravo IJG, de Almeida Macedo WA, de Sousa EMB. Mesoporous silica materials functionalized with folic acid: preparation, characterization and release profile study with methotrexate. Journal of Sol-Gel Science and Technology. 2016;77(1):186-204.

35. Knežević NŽ, Durand JO. Targeted treatment of cancer with nanotherapeutics based on mesoporous silica nanoparticles. ChemPlusChem. 2015;80(1):26-36.

36. Sing KS. Reporting physisorption data for gas/solid systems with special reference to the determination of surface area and porosity (Recommendations 1984). Pure and applied chemistry. 1985;57(4):603-19.

37. Yang P, Quan Z, Lu L, Huang S, Lin J. Luminescence functionalization of mesoporous silica with different morphologies and applications as drug delivery systems. Biomaterials. 2008;29(6):692-702.

38. Yang K-N, Zhang C-Q, Wang W, Wang PC, Zhou J-P, Liang X-J. pH-responsive mesoporous silica nanoparticles employed in controlled drug delivery systems for cancer treatment. Cancer biology & medicine. 2014;11(1):34-43.

39. Bruschi ML. Strategies to modify the drug release from pharmaceutical systems: Woodhead Publishing; 2015.

40. Jin S, Liu M, Chen S, Gao C. A drug-loaded gel based on polyelectrolyte complexes of poly (acrylic acid) with poly (vinylpyrrolidone) and chitosan. Materials Chemistry and Physics. 2010;123(2):463-70.

41. Daryasari MP, Akhgar MR, Mamashli F, Bigdeli B, Khoobi M. Chitosan-folate coated mesoporous silica nanoparticles as a smart and pH-sensitive system for curcumin delivery. RSC Advances. 2016;6(107):105578-88.

42. Li J, Zheng L, Cai H, Sun W, Shen M, Zhang G, et al. Polyethyleneimine-mediated synthesis of folic acid-targeted iron oxide nanoparticles for in vivo tumor MR imaging. Biomaterials. 2013;34(33):8382-92.